Journal of Structural Geology 33 (2011) 644–661

Contents lists available at ScienceDirect

Journal of Structural Geology

journal homepage: www.elsevier.com/locate/jsg

Variation in fracture patterns in damage zones related to strike-slip faults interfering with pre-existing fractures in sandstone (Calcione area, southern Tuscany, Italy)

Andrea Brogi*

University of Siena, Department of Earth Sciences, Via Laterina 8, 53100 Siena, Italy

ARTICLE INFO

Article history:
Received 26 March 2010
Received in revised form
3 December 2010
Accepted 13 December 2010
Available online 21 December 2010

Keywords:
Strike-slip faults
Scaling relation
Fracture pattern
Fault linkage
Kinematics analyses

ABSTRACT

This paper deals with the effects of pre-existing fractures on the development of damage zones related to meter and decameter strike-slip faults, which affected Late Oligocene-Early Miocene sandstone in the Calcione area, southern Tuscany (Italy). Strike-slip faults dissected rock masses locally affected by pervasive, pre-existing fractures related to previous deformational events. Two different domains were identified: rock masses affected and unaffected (or relatively unaffected) by pre-existing fractures. Strike-slip faults affecting the two domains made it possible to compare the different configurations of fracture patterns related to isolated or interacting fault segments. New data is provided on scaling relations between: i) fault length and the length of related fractures; ii) mean step length and width for over-stepping fault segments; iii) angular values at the intersection of the fault plane and related fractures. Scaling relations obeyed a positive power law for faults dissecting sandstone unaffected by pre-existing fractures. On the contrary, no scaling relations were recognized for faults dissecting sandstone affected by pre-existing fractures. The development of strike-slip faults on rock masses affected by pre-existing fractures can simulate splays apparently related to faulting. Three main points were categorized for detecting deceptive cases. There is a real chance of a deceptive fracture pattern if: i) the angular values at the intersection of the fault and its fractures (mode I opening fracture) exceed 50° in the wall damage zone; ii) the scaling relation between fault length and maximum fracture length does not fit a power law; iii) fractures acted as shear fractures. The resulting framework provides additional data for understanding the development and architecture of strike-slip faults.

1. Introduction

Strike-slip faults accommodating horizontal displacements in response to plate movements are common structures in the Earth's crust (Sylvester, 1988). Their occurrence reflects the complex settings and histories of horizontal slip restricted to intraplates (e.g. transcurrent faults) or extended to plate margins (e.g. transform faults). Strike-slip faults can develop at different scales (Storti et al., 2003) and play a fundamental role in the rise of magma and volcanic eruption (Ventura et al., 1999; Adiyaman and Chorowicz, 2002; Garcìa-Palomo et al., 2004; Acocella and Funiciello, 2005; Storti et al., 2006; Tibaldi et al., 2008; Brogi et al., 2010), basin development (Aydin and Nur, 1982; Mann et al., 1983; Biddle and Christie-Blick, 1985; Woodcock, 1986; Cakir et al., 1998), earthquake activity (Segall and Pollard, 1983; Sibson, 1985, 1986; Harris et al., 1991; Albarello et al., 2005; Corti et al., 2005; Delacou et al., 2005; Drukpa et al., 2006; Rodgers and Little, 2006; Catchings et al., 2009; Abou Elenean et al., 2010), fluid migration and consequent formation of ore deposits (Wibberley and Shimamoto, 2003; Cembrano et al., 2005; Bellot, 2008), oil and gas traps (Aydin, 2000; Odling et al., 2004; Lazar et al., 2006; Dong et al., 2008), and so on. Strike-slip faults and related fracture networks are therefore widely studied for insights into fault zone geometry, dynamics and evolution. During tectonic investigations, reconstructing the kinematics of strike-slip faults is fundamental to obtain constraints of the structural setting and tectonic evolution of a region. Recognizing kinematic indicators on the main slip surfaces is crucial, but in some cases unfeasible. However, critical information can be obtained from minor structures developing in the fault core (Billi et al., 2003; Berg and Skar, 2005; Agosta and Aydin, 2006; Brogi, 2008; Bastesen et al., 2009; Molli et al., 2009) and damage zones (Riedel, 1929; Hancock, 1985; Petit, 1987). Several authors

* Tel.: +39 0577 233971; fax: +39 0577 233938.
E-mail address: brogiandrea@unisi.it.

0191-8141/$ – see front matter © 2010 Elsevier Ltd. All rights reserved.
doi:10.1016/j.jsg.2010.12.008

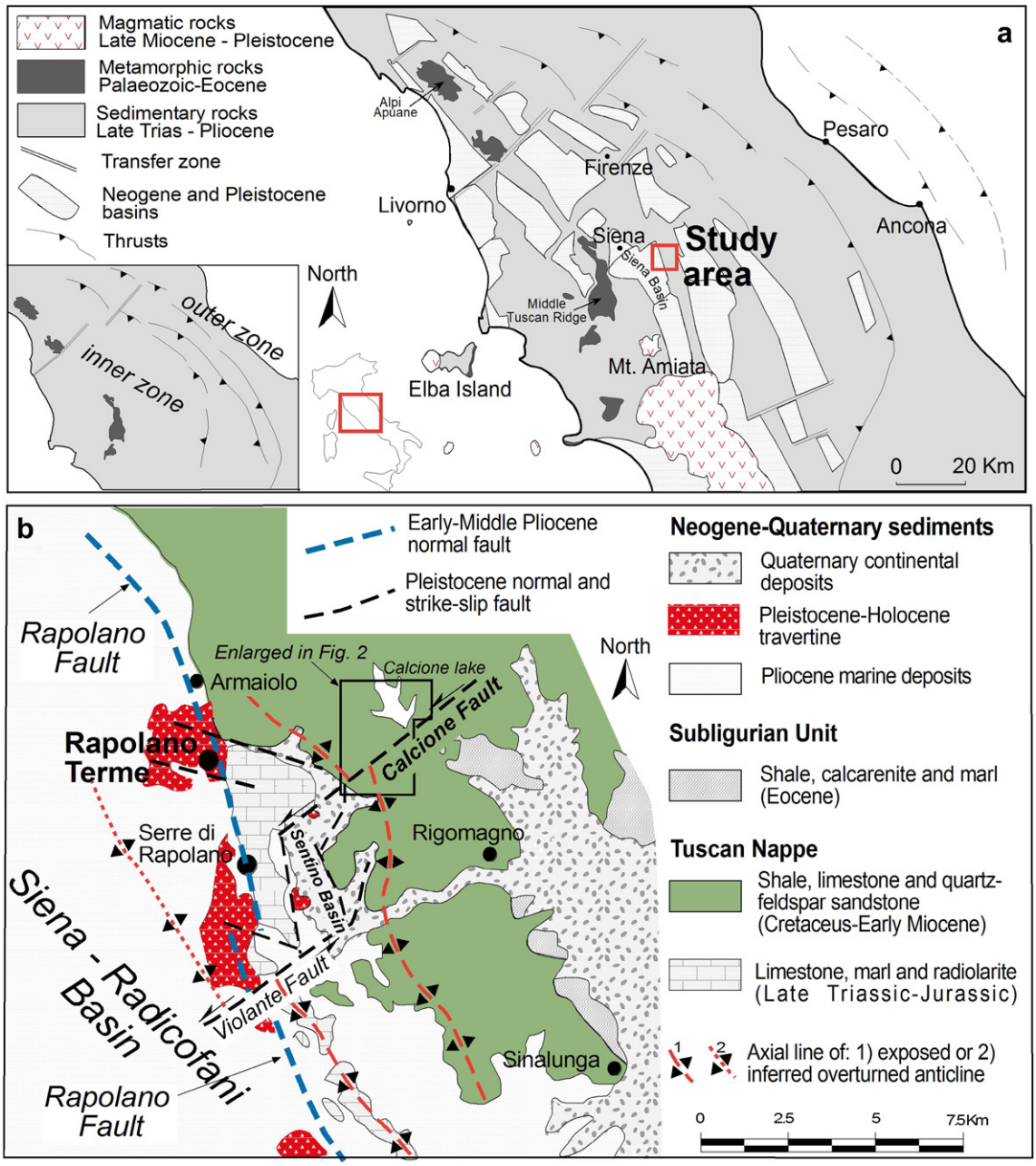

Fig. 1. a) Geological sketch-map of the northern and central Apennines (southern Tuscany, northern Latium and northern Tyrrhenian Sea) and location of the study area; b) geological map of the eastern side of the Siena Basin and Rapolano Terme region where the Calcione area is located. The main structural elements are also indicated and discussed in the text. Modified after Carmignani and Lazzarotto (2004).

(Martel et al., 1988; Mollema and Antonellini, 1999; Kim et al., 2003, 2004; Myers and Aydin, 2004; Flodin and Aydin, 2004; de Joisseneau and Aydin, 2007, 2009) have described splays forming a dense and well-connected damage zone around strike-slip faults. Splays may enhance fault zone permeability with great impact on fluid flow along fault zones and could have a strong influence on the evolution of the fault zones (McGrath and Davison, 1995; Davatzes and Aydin, 2003; Devatzes et al., 2003; Martel et al., 1988; Kelly et al., 1998; Myers and Aydin, 2004; Flodin and Aydin, 2004a; Kim et al., 2004). Splay arrangements in plain view provide precious information on strike-slip fault kinematics. In particular, their lateral sense of movement can be reconstructed on the basis of (Martel, 1990; Peacock and Sanderson, 1991, 1995; Cooke, 1997; Willemse and Pollard, 1998; Kim et al., 2003, 2004; Myers and Aydin, 2004; de Joisseneau and Aydin, 2007): i) angular relationships between the main fault plane and the fractures formed in the damage zone; ii) the geometrical setting of fractures developing at tip zones; iii) the attitude of minor structures in linkage zones between two main fault segments.

Although the geometrical relationships between the fault plane and related fractures provide unambiguous information for deducing the lateral sense of movement, Flodin and Aydin (2004) documented several cases of strike-slip faults in sandstone that could be misinterpreted. They stressed that care should be taken in interpreting their kinematics only on the basis of fault-fracture angular relationships. Indeed, the configuration of pre-existing structures can influence fault growth, as well as the geometric pattern of related fractures. Misinterpretation of the fracture

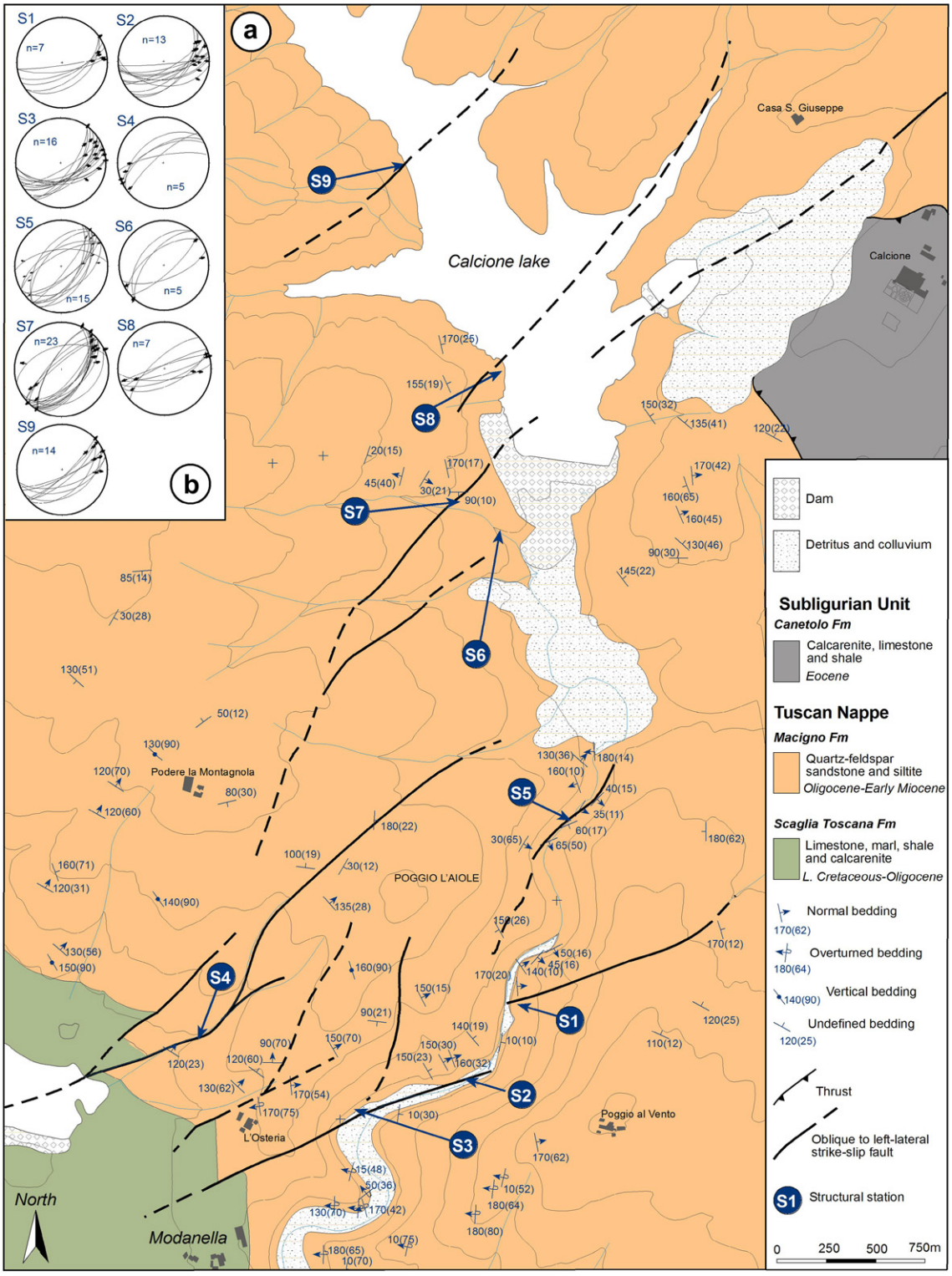

Fig. 2. a) Geological map of the Calcione area. The structural stations of the left-lateral oblique and strike-slip faults belonging to the Calcione fault zone are also reported. b) Stereographic diagrams (lower hemisphere, Schmidt diagram) showing faults and striae from the structural stations reported in the figure a.

network around faults may lead to incorrect evaluation of strike-slip lateral sense of movement, invalidating a structural reconstruction.

This paper is concerned with the effects of pre-existing fractures on the growth of strike-slip faults and related damage zones. The architectural features of several strike-slip fault zones affecting Late Oligocene-Early Miocene sandstone exposed in central Italy (Northern Apennines, Calcione area, Fig. 1), combined with field studies and published data sets for other faults around the world, were analyzed. The resulting framework provides additional data for insights into the development and architecture of strike-slip faults, also focusing on muddled fractures that may lead to incorrect kinematic reconstructions.

2. Geological outline

The Calcione area is located in the inner Northern Apennines (southern Tuscany), close to the Rapolano Terme low-enthalpy geothermal region (Fig. 1b). The Late Triassic-Early Miocene Tuscan Nappe succession, unconformably overlaid by Pliocene marine sediments and Pleistocene continental deposits, broadly crops out (Brogi, 2004). The Tuscan Nappe is the deepest non-metamorphic tectonic unit of the Northern Apennines, stacked during the Late Oligocene-Early Miocene (Carmignani et al., 2001).

Since the Early-Middle Miocene, the inner Northern Apennines has been affected by extensional tectonics (Carmignani et al., 1994; Brogi et al., 2005 and references therein) which produced thinning of the continental crust and lithosphere (20–24 km and 30–50 km, respectively) and development of widespread structural depressions filled by continental and marine sediments (Martini and Sagri, 1993; Brogi and Liotta, 2008). Extension was accompanied by magmatism (Serri et al., 1993; Peccerillo et al., 2001) which led to emplacement of magmatic intrusions at depth (Dini et al., 2002, 2005, 2008; Rossetti et al., 2008) and volcanic eruptions. The whole inner Northern Apennines is now characterized by a geothermal anomaly estimated to have an average heat-flow of 150 mW/m^2, reaching 1000 mW/m^2 in the Larderello–Travale geothermal area (Della Vedova et al., 2001).

The Calcione area is located in the eastern side of a broad Neogene structural depression, known as the Siena-Radicofani Basin (Martini and Sagri, 1993) (Fig. 1b). This structural depression was filled by Neogene and Quaternary marine to continental sediments (Bossio et al., 1993; Liotta, 1996; Bonini and Sani, 2002; Aldinucci et al., 2007). A regional Pliocene normal fault, known as the Rapolano Fault (Costantini et al., 1982), NNW-SSE striking and west-dipping, separates the Pliocene sediments filling the Siena-Radicofani Basin from the Tuscan Nappe Mesozoic carbonate and siliceous formations (Fig. 1b). Widespread geothermal manifestations, such as thermal springs (39 °C), travertine deposits and gas vents (mainly CO_2, H_2S, Etiope et al., 2005) are structurally controlled. They are distributed along the traces of Pleistocene faults (Brogi, 2008; Brogi and Capezzuoli, 2009) and the Rapolano Fault (Cipriani et al., 1972; Minissale et al., 2002), mainly where the latter was dissected by near-orthogonal Middle-Late Pleistocene transtensional faults (Brogi, 2004; Brogi et al., 2009).

3. The study area

The faults analyzed are minor structures belonging to a major SW-NE striking left-lateral strike-slip fault system, Pleistocene in age, related to the development of the Sentino Basin (Fig. 1b). This basin consists of a Late Pliocene-Pleistocene structural depression developed in a linkage zone between two main left-lateral transtensional faults (Brogi et al., 2002): the Calcione fault and the Violante fault (Fig. 1b). On the basis of mapping considerations, the Calcione and Violante faults produced a horizontal offset of a few hundred meters. They dissected two regional east-verging overturned anticlines (Fig. 1b) that strike NNW-SSE (Aqué and Brogi, 2002; Brogi et al., 2002). These folds developed during the Early-Middle Miocene and characterize the whole Rapolano-Monte Cetona ridge (Losacco and Del Giudice, 1958; Passerini, 1964; Lazzarotto, 1973). Strike-slip faults kinematics were defined by structural analyses of key outcrops, mainly in the Violante fault zone (Brogi et al., 2009). This fault dissected Late Triassic-Jurassic carbonate rocks, producing large-volume hydrothermal fluid circulation. Fluid flow across the fault zone gave rise to hydrothermal alteration and travertine deposition coeval with the latest stage of fault activity, related to the Late Pleistocene (Brogi et al., 2009).

The Calcione fault zone affected the Late Oligocene-Early Miocene Tuscan Nappe turbiditic succession (Macigno Fm, Cornamusini, 2002), composed of quartz-feldspar-micaceous sandstone with interbedded siltite beds. In the study area, the Calcione fault zone consists of a wide, SW-NE striking, brittle shear zone characterized by fault segments organized in en-échelon geometrical configuration (Fig. 2). Minor strike-slip to oblique-normal faults, WSW-ENE and W-E trending, are associated with the main fault segments shown in Fig. 2b, and are particularly exposed along the southwestern shore of Lake Calcione (Fig. 2).

The turbiditic succession recorded a polyphase tectonic history (Elter and Sandrelli, 1994; Bonini, 1999) during Tertiary structural evolution of the inner Northern Apennines (Carmignani et al., 1994; Liotta et al., 1998). The Pleistocene strike-slip faults superimposed on previously deformed rock masses, locally characterized by intense deformation, are described in the next section.

3.1. Nomenclature and methodology

In order to describe the geometry and architecture of the analyzed faults and related minor structures, the nomenclature proposed by Peacock et al. (2000) was used. According to this nomenclature, the term fracture includes all planar or semi-planar discontinuities affecting rock masses: i) joints (Pollard and Aydin, 1988; Pollard and Segall, 1987); ii) deformation bands (Aydin, 1978); iii) slip surfaces (Aydin and Johnson, 1978, 1983) including faults.

The faults are exposed for tens of meters along the raised lakeshore and its surroundings (Fig. 2). The rest of the area is characterized by thick forest, where the faults can only be recognized in very limited and scattered outcrops, mainly along stream incisions. Kinematic analysis was performed in structural stations (Fig. 2).

Sixteen minor fault zones related to the major Calcione fault (Figs. 1 and 2) were considered. Five faults dissected sandstone affected by pre-existing NW-SE striking fractures (see next section); eleven faults displaced rock masses where the bedding was the most pervasive pre-existing structure.

Measurements were taken on the fault zone in order to collect a data set on: 1) the geometric pattern of the fault zones; 2) the angular relationships between fractures and fault planes; 3) fault kinematics.

The geometrical patterns of the fault zones were reconstructed directly on the outcrops by detailed mapping. Boxes delimited by metric strings were used to map fault portions. The length and strike of the box sides were measured and recorded on graph paper at scale 1:100. All structural elements occurring within a box were analyzed and measured. If necessary, the box side was reduced to 1 m; all structures within the square meter were redrawn using photographs. All linear measurements had a precision of about 2%.

The angular relationships between fractures and fault planes were measured directly on the outcrops where 3D exposures could also be recognized.

The kinematics of the faults were inferred by analysis of the indicators recognized on the fault planes. In fact, all fault planes have sub-horizontal striations indicating dominant strike-slip movements. Strike and dip values of the fault planes were reported in stereographic diagrams coupled with the pitch angles of the striations (Fig. 2).

3.2. Fault/fracture angular relationships versus lateral sense of movement

It is accepted that fault/fractures angular relationships are a useful indicator for deducing the lateral sense of movement of strike-slip faults (Kim et al., 2004 for a review). In particular, this lateral sense of movement is indicated by the acute angles formed

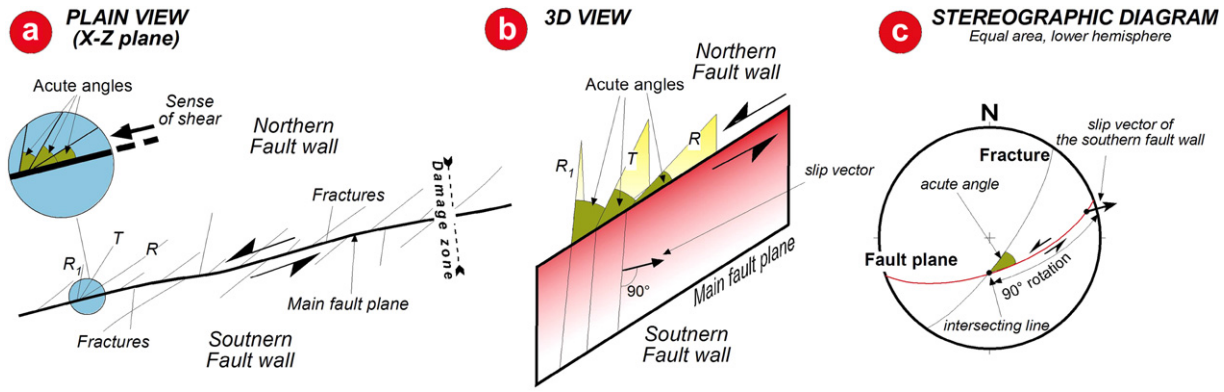

Fig. 3. Cartoon showing the conceptual scheme reconstructing the lateral sense of movement of a strike-slip fault through the fault/fractures relationships. See the text for more details.

at the intersection between R-, R_1-, and T-type discontinuities and the fault plane (Cloos, 1928; Riedel, 1929; Tchalenko, 1970; Bartlett et al., 1981; Petit, 1987; Wookcock and Schubert, 1994; Davis et al., 2000) in the x–z plane of the finite strain ellipsoid (Fig. 3a). In several cases, the slip vector can be determined by a geometric construction: T-, R- and R_1-type discontinuities intersect faults along lines perpendicular to the slip direction (Sibson et al., 1988; de Ronde et al., 2001; Wilkins et al., 2001; Miller and Wilson, 2004) as illustrated in Fig. 3b. Although this geometric construction can be considered true in most cases, Blenkinsop (2008) described anomalous conditions: the geometric construction shown in Fig. 3b cannot be considered true for: (i) reactivated faults, (ii) faults in multiple sets, and (iii) Healy theory faults (Healy et al., 2006). Nevertheless, in nearly every case the slip vector is indicated by the acute angles formed at the intersection between R-, R_1- and T-type fractures and the fault plane (Fig. 3 a–b), or by the obtuse angle formed at the intersection between a P-type fracture and the fault plane. The orientation of the slip vector can be calculated using stereographic projections (Schmidt diagram, lower hemisphere) (Fig. 3c): the point defined by the intersection between the fault plane and fracture great circles enables reconstruction of strike and dip values of the line defined by the fault/fracture intersection. Furthermore, strike and dip values of the slip vector can be calculated at 90° from the fault/fracture intersection point along the great circle of the fault plane (Fig. 3c).

3.3. Protolith fabric and pre-faulting structures

Protolith consists of alternating beds of arkosic sandstone and subordinate amounts of siltite (Fig. 4), belonging to the Late Oligocene-Early Miocene Macigno Fm (Cornamusini, 2002), interpreted as a thick foredeep turbiditic succession formed during the building of the Northern Apennines chain. The sandstone beds have thicknesses ranging from several centimeters to 3 m. Sandstone

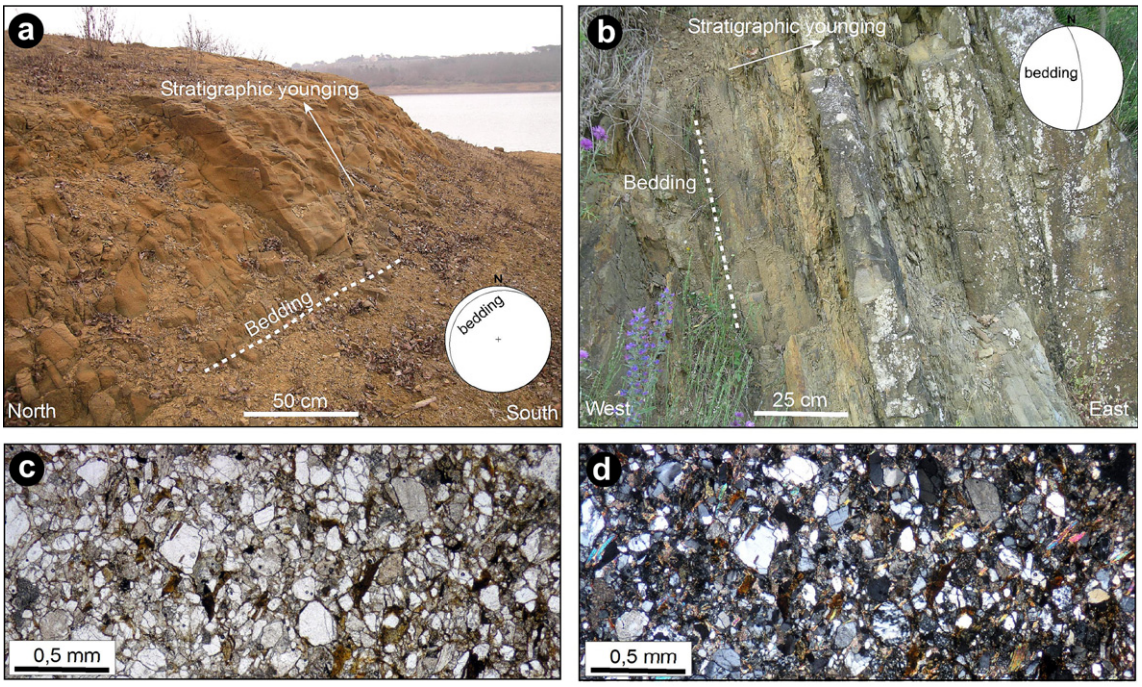

Fig. 4. Lithological features of the Late Oligocene-Early Miocene sandstone turbiditic succession (Macigno Fm) exposed in the study area; a) fining upward quartz-feldspar sandstone beds, 2m thick, exposed close to the Calcione lake; b) centimeter fining upward sandstone beds with interbedded siltites; c) and d) photomicrographs (plane polarized and crossed nicols light, respectively) of the quartz-feldspar sandstone mainly composed of quartz, feldspar, white mica, lithics (metamorphic rocks) and fe-oxides.

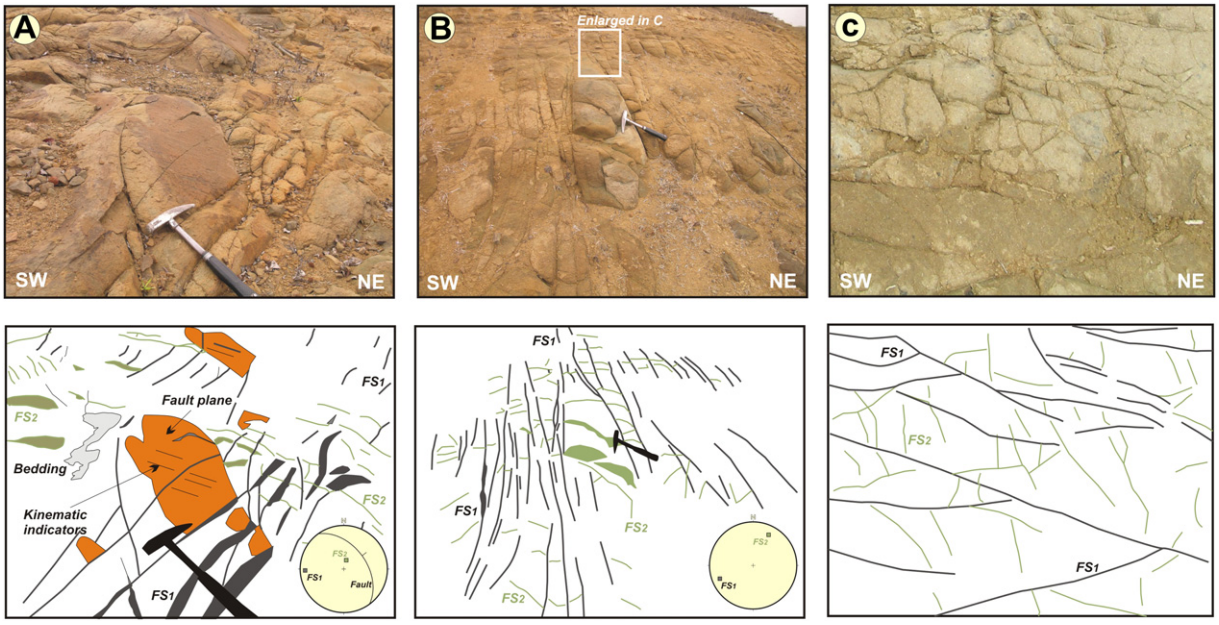

Fig. 5. Photographs and related line-drawings of rock masses deformed before the strike-slip faults. A) Normal fault with decimeter offset crossed by mode I fractures belonging to the FS1 Fracture system. B) and C) Fracture network related to FS_1 and FS_2 fracture systems. See the text for more details.

beds range from moderately to poorly sorted and contain a considerable quantity of quartz grains (mono and polycrystalline), feldspar grains (plagioclase and k-feldspar), white mica and chlorite grains, and crystalline lithics mainly consisting of granitoid and metamorphic rock fragments (Fig. 4c–d). The cement is mainly argillaceous-phyllosilicatic or composed of quartz, generally constituting overgrowths on quartz grains. Siltite beds do not exceed 10 cm in thickness. They show pervasive fissility mainly due to very abundant phyllosilicate grains.

The most recurrent small-scale structures preceding the strike-slip faults were normal faults (NFs) with decimeter to meter offsets. sub-vertical, pervasive and sub-parallel fractures ascribed to two different main fracture systems (FSs) are also present. Cross-cutting and abutting relationships between the different structures are used to define their relative chronology. Fig. 5 illustrates the geometric relationships between NFs and different FSs as detectable on the outcrops. The FSs consist of mode I opening fractures generally characterized by typical surface morphology, such as hackle marks defining plumose structures (Pollard and Aydin, 1988). In a few cases the fractures were reactivated as shear fractures (see the next paragraph), coherently with the stress fields, giving rise to strike-slip faults.

FS_1 consists of a fracture set composed of sub-parallel and sub-vertical fractures, locally spaced up to 10 fractures per meter (Fig. 6). These fractures discontinuously affect the whole study area. Fractures are concentrated in wide, discontinuous domains, where they are the most pervasive surfaces together with the bedding. In contrast, the bedding, nearly sub-horizontal or gently inclined toward E and NE, is the main structure characterizing the domains not affected, or relatively unaffected, by fractures. Domains affected by FS_1 are distributed throughout the whole study area, giving the Calcione sandstone a widespread structural feature. Fractures strike N120° to N180° as reported in the stereographic diagrams of Fig. 6.

Normal faults predated FS_1 (Fig. 5). The normal faults are characterized by average N130°–140° strike and consist of minor structures associated with the Early-Middle Pliocene Rapolano

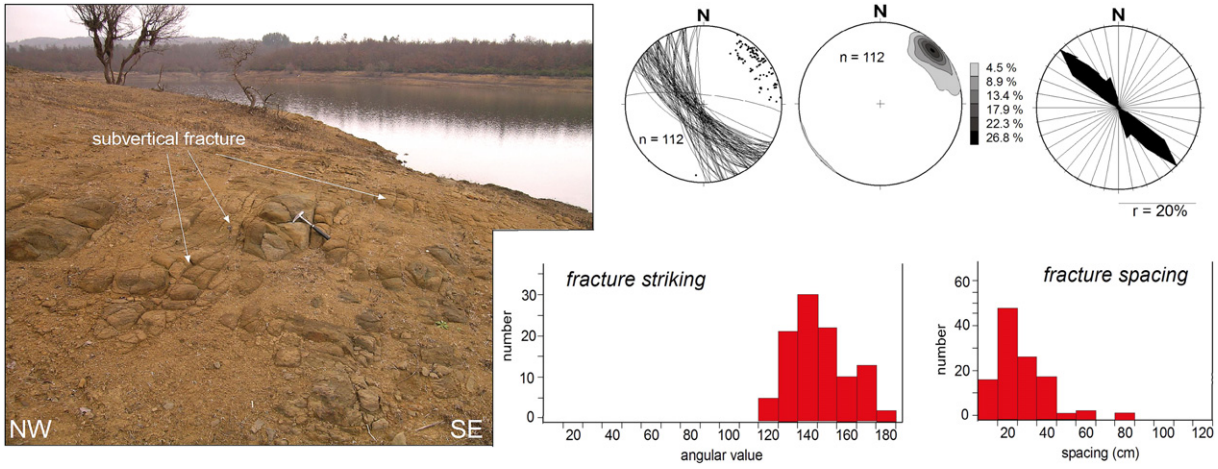

Fig. 6. Sandstone affected by pervasive and sub-vertical fractures related to a deformational event pre-dating strike-slip faults, see the text for more details. Histograms, stereplots (lower hemisphere, Schmidt diagram) and rose diagram illustrate the geometrical features of the fractures.

Fault system (Fig. 1b). Minor normal faults in the Calcione area are characterized by decimeter to meter offsets and therefore cannot be mapped. Kinematic indicators on the fault planes, consisting of mechanical striation and rare quartz-fibers coupled with iron-hydroxides, indicate dominant dip-slip displacement (pitch ranging from 70° to 90°, Fig. 5).

FS_2 fractures gave rise to clustering within rock lithons defined by FS_1 structures (Fig. 5). Their intersection geometries are mainly Y- and T-type (Hancock, 1985; Pollard and Aydin, 1988). FS_1–FS_2 abutting relationships suggest a later origin of FS_2 with respect to FS_1 structures. Their origin could be related to variations in stresses around FS_1 fractures during their formation, or to progressive brittle deformation. FS_2 fractures range from 5 to 45–50 cm in length and from N110° to N15° in strike.

4. Strike-slip fault zone geometry and kinematics

Fault zone geometry and the associated fracture pattern show different features depending on two main facts: i) pre-existing fractures in the rock masses; ii) angular relationships between strike-slip faults and pre-existing fractures. Systematic structural analysis and field measurements of key outcrops mainly enabled reconstruction of 2D structural geometries.

4.1. Strike-slip faults in sandstone unaffected by pre-existing fractures

Strike-slip faults dissecting sandstone unaffected, or relatively unaffected, by pre-existing fractures are characterized by fault zones not exceeding 10 m in width. The faults have displacements exceeding 2 m, even if their exact offset cannot be defined with precision, due to a lack of clear markers.

According to most authors (Chester and Logan, 1986; Chester et al., 1993; Caine et al., 1996; Billi et al., 2003) the fault zones can be partitioned into two main components: the fault core and the damage zone.

The fault core mainly accommodated the maximum shear deformation. It consists of a structurally complex and lithologically heterogeneous cataclastic rock, up to 25 cm wide (Fig. 7a) and is mainly composed of cemented angular to sub-angular comminuted quartz grains, embedded in a very fine-grained phyllosilicate-rich matrix, locally entraining parts of host rocks. Locally, crush breccia (Sibson, 1977) with clasts ranging from 1 to 3 cm (Fig. 7b–d) is the dominant fault rock. The phyllosilicate-rich matrix consists of Fe-hydroxides and a mixture of phyllosilicates (largely muscovite and chlorite), mainly derived from comminution of grains forming the host rocks (Fig. 8). The limit between fault core and damage zone is

Fig. 7. Strike-slip fault exposed close to the Calcione lake; a) particular of the northern wall damage zone and fault core containing the fault plane; b) detail of the fault core composed of centimeter clasts dispersed within a clayey matrix; c) millimeter tick clayey gouge; d) crush breccias characterizing a part of the fault core; e) oblique mechanical striae along the fault plane; f) calcite fibers indicating left-lateral strike-slip kinematics.

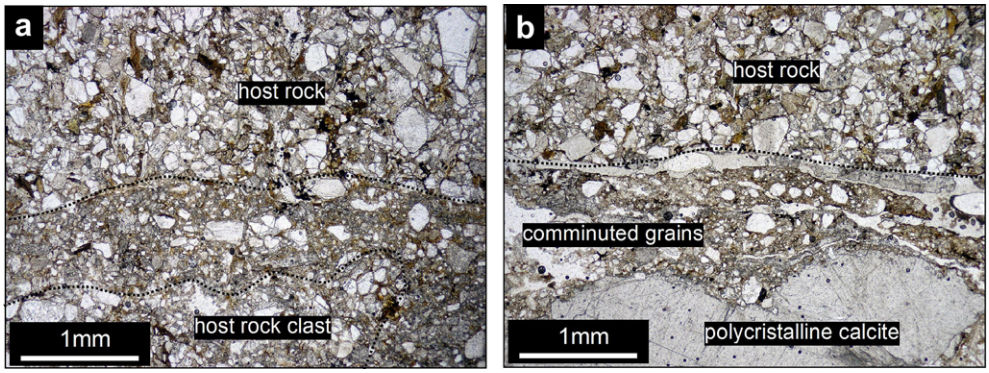

Fig. 8. Microphotographs (plane polarized light) of sandstone involved in faulting; a) detail of the fault core where comminuted grains gave rise to the phyllosilicate-rich matrix; b) neoformational calcite attesting fluid migration along the fault zone.

locally defined by a highly polished and striated (slickenside) slip surface, occasionally characterized by calcite fiber growth (Fig. 7e–f).

The damage zone is composed of a discrete zone of the host rock containing fractures distributed in variable volumes. En-échelon fractures characterizing the fault damage zones are called splays, also known as wing, tail, kink, horsetail and branch cracks, and consist of dominantly opening-mode (mode I) fractures formed in response to slip across faults in brittle rocks such as sandstone (Cruikshank et al., 1991; Myers and Aydin, 2004).

Different features characterize the damage zones depending on their location with respect to the fault plane (McGrath and Davison, 1995; Kim et al., 2003; According to Kim et al. (2004), damage zones can be divided into three main types: i) wall, ii) linking and iii) tip damage zones (Fig. 9a).

The wall damage zones (distributed damage zones in Kim et al., 2003) are narrow zones characterized by en-échelon fractures showing similar length and spacing (Fig. 10a). The length, spacing and strike of the fractures were measured for each strike-slip fault. In general, fractures are concentrated in meter-wide domains having high deformation density, characterized by 12 fractures per meter (Fig. 11), separated by intermediate domains where the density of fractures is lower: 2–3 fractures per meter (Fig. 11). On the whole, fractures formed at 25–42° to the main fault plane (Fig. 10a). Some fractures have sigmoidal shape, whereas some of which evolved into synthetic faults (sheared fractures) showing associated minor fractures. In several cases, fractures in the wall damage zones isolated lithons of host rocks, preserving protolith fabric.

Linking damage zones consist of highly fractured zones connecting two segments of strike-slip faults. They developed in releasing overstep zones or in understepping co-planar fault segments (Fig. 9a). The releasing overstep zones are characterized by fractures connecting the two faults segments (Fig. 10b). Fractures are at 30°–50° to the overstepping fault segments and mostly

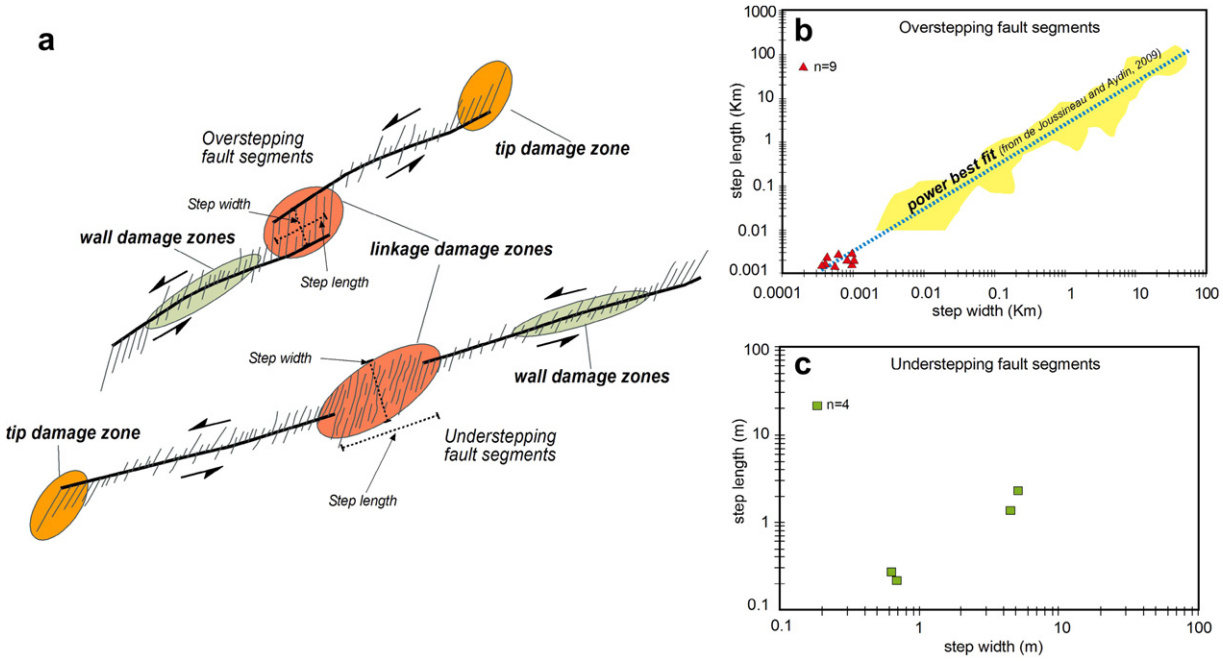

Fig. 9. a) Cartoon showing different linkage patterns between two main left-lateral strike-slip fault segments as recognized in the study area (terminology from Kim et al., 2003, 2004). b) Relationships between step width and step length for overstepping strike-slip faults from the Calcione area (red triangles) integrated with data published (yellow field) by other authors (Aydin and Nur, 1982; Wesnousky, 1988; Stirling et al., 1996; Sieh and Natawidjaja, 2000; Le Pichon et al., 2001; Jachens et al., 2002; Maruyama and Lin, 2002; Walker and Jackson, 2002; Tatar et al., 2004; Fu and Awata, 2006; Nemer and Meghraoui, 2006; de Joussineau and Aydin, 2009). c) Relationships between step width and step length for understepping strike-slip faults from the Calcione area. (For interpretation of the references to colour in this figure legend, the reader is referred to the web version of this article).

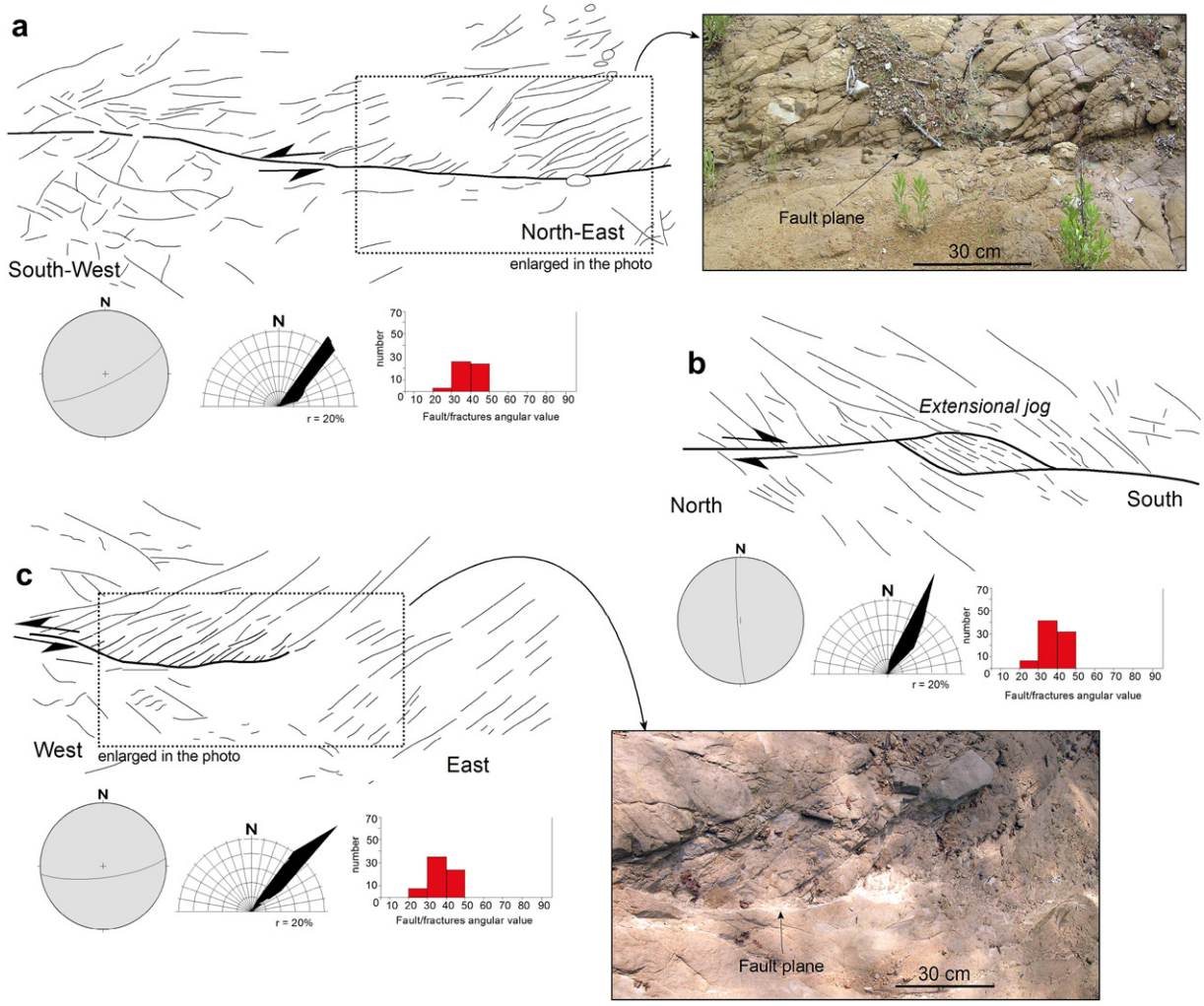

Fig. 10. Different damage zones geometrical features associated to the strike-slip faults recognized in the study area; a), b) and c) are different cases discussed in the text. The diagrams illustrate, from the left: stereographic diagram (lower hemisphere, Schmidt diagram) showing the great circle of the fault plane; rose diagram of the fractures in the damage zone; histogram showing the angular values at the intersection of fault planes and their fractures.

prove affected by hydrothermal alteration, indicating the major role of linkage zones for fluid flow along fault zones. Linking damage zones between understepping fault segments are characterized by en-échelon fractures parallel to those formed in the wall damage zones. They can be compared with the antithetic faults described by Kim et al. (2003). The relationships between step width and step length of overstepping and understepping fault segments were also investigated for measurable faults. Little data was obtained and was added to that of other places around the world. In the diagrams of Fig. 9b mean step length and width for overstepping fault segments

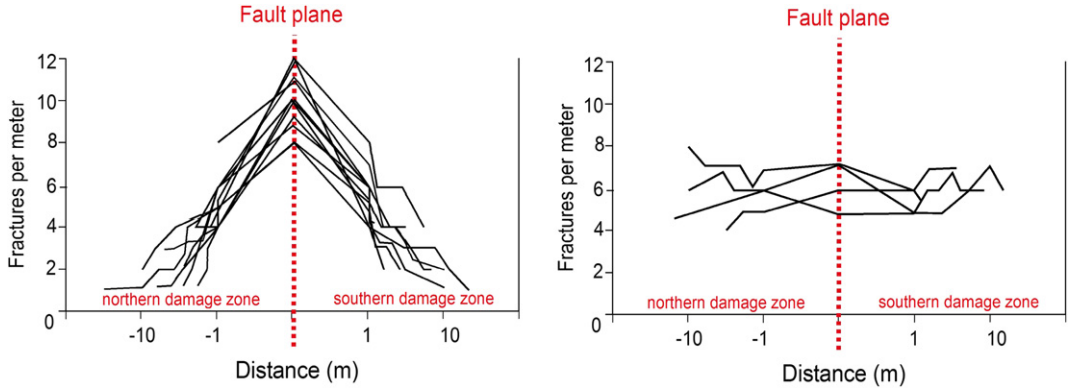

Fig. 11. Diagrams illustrating the fractures density for the analyzed faults. Left) Fractures density measured for the strike-slip faults dissecting sandstones unaffected by pre-existing fractures. Right) Fracture density measured for the strike-slip faults dissecting sandstones affected by pre-existing fractures.

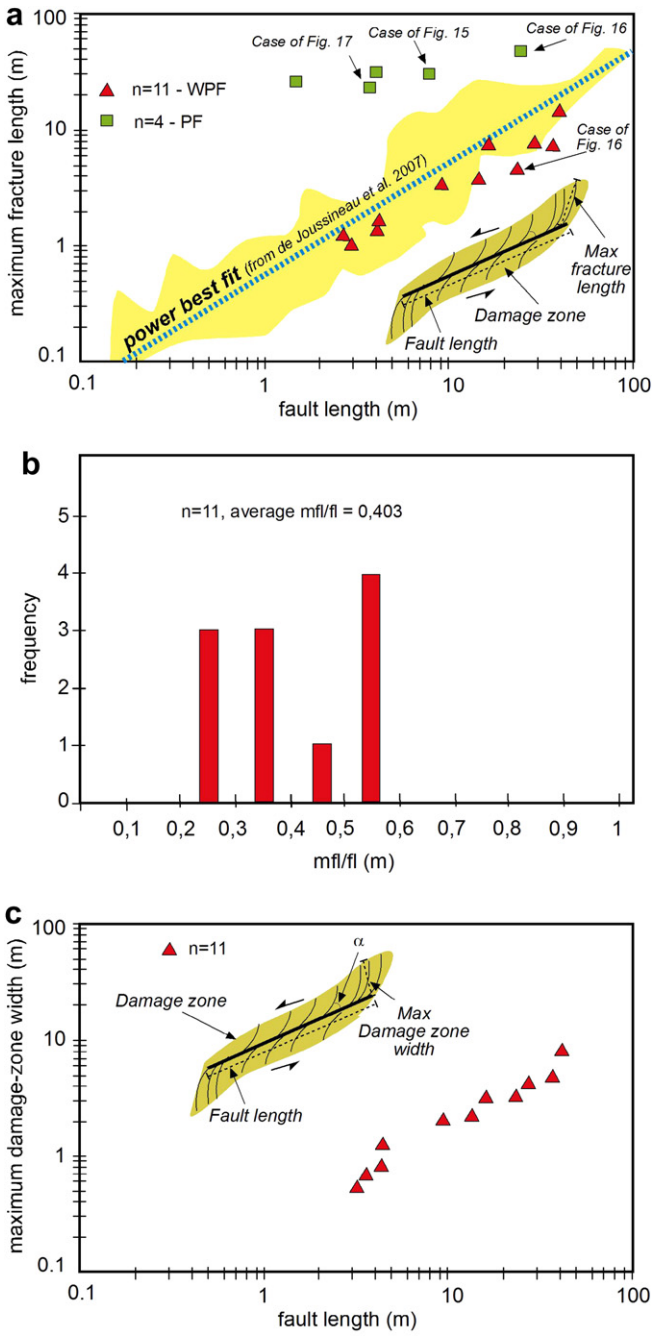

Fig. 12. a) Relationships between maximum fracture length and related fault length from the Calcione area (red triangles and green squares) integrated with data published (yellow field) by other authors (de Joisseneau et al., 2007); WPF: data for faults affecting rock masse not affected by pre-existing fractures; PF: data for faults affecting rock masse with pre-existing fractures. b) Frequency *vs* ratio of maximum fracture length (mfl) to related fault length (fl). c) Relationships between the maximum width of the (half) damage zone and the fault length. (For interpretation of the references to colour in this figure legend, the reader is referred to the web version of this article).

were plotted on the *y* and *x* axis, respectively. The collected data aligns well with the best fit reported by de Joisseneau and Aydin (2009) describing a quasi-linear positive power law relationship:

$$Y = 2.69 \times x^{0.97}$$

with $R^2 = 0.93$.

Mean step length and width for understepping fault segments are plotted in Fig. 9c. This data, too, is distributed along a positive power law trend but the equation that defines the power law cannot be reconstructed due to a shortage of data.

Tip damage zones mainly consist of asymmetric damage zones characterized by fractures at 35°–50° to the fault plane (Fig. 10c), classifiable as horsetail splays described by Kim et al. (2004).

Geometrical relationships between faults and their associated fractures were also investigated for several faults. In fact, eleven strike-slip left-lateral faults ranging from 2 to 40 m in length are well exposed, enabling their geometry to be analyzed. Relationships between fault lengths (fl) and the length of their longest fractures (maximum fracture length-mfl) in damage zones were considered and compared with data from the literature (e.g. de Joisseneau et al., 2007). The results are reported in Fig. 12a and are consistent with the power law defined by de Joisseneau and Aydin (2007):

$$\mathrm{mfl} = 0.54 \times \mathrm{pfl}^{0.95}$$

with $R^2 = 0.79$. The average mfl/fl obtained was 0.403 (Fig. 12b) indicating that the common value for maximum fracture length of the damage zone is 40% of the fault length.

The fault plane and related fractures in the damage zones intersect at 38° (α) on average. This angular value coupled with maximum fracture length (mfl) made it possible to calculate the maximum width of the damage zone (WDZmax) through the following equation:

$$\mathrm{WDZ_{max}} = \mathrm{mfl} \times \sin\alpha$$

The relationships between fault length and the maximum width of their damage zones are reported in Fig. 12c.

Fig. 13A illustrates stereographic diagrams comparing the fault/fracture intersection and the slickenline for individual faults in order to reconstruct their angular relations (cf. Blenkinsop, 2008). The geometrical relations and angular values will be discussed later.

4.2. Strike-slip faults interfering with pre-existing fractures

Strike-slip faults dissecting sandstone affected by pre-existing fractures are characterized by atypical geometrical patterns. For example, the length of the faults and the length of their apparent longest fractures show anomalous relationships with respect to the scaling relation of rock masses not affected (or relatively unaffected) by pre-existing fractures (Fig. 12a). The fracture network in fault damage zones may also prove very complicated, as pre-existing fractures could influence the trajectories of fractures formed later. In fact, fractures related to faulting form at low angles to the fault plane and abut or curve into the trace of the pre-existing fracture (Fig. 14).

Depending on the angular relationships between pre-existing fractures and the strike-slip faults, different geometrical patterns were created. Two main cases have been selected: i) strike-slip faults superimposed on near-orthogonal pre-existing fractures; ii) strike-slip faults superimposed obliquely on pre-existing fractures.

Figs. 15 and 16 illustrate examples of strike-slip faults superimposed on near-orthogonal, dominant pre-existing fractures. Such faults strike N70°-80° and are superimposed on near-orthogonal (N140°-150° striking) pre-existing fractures of FS_1.

Fig. 15 shows a strike-slip fault characterized by a very thin fault core composed of a millimeter-thick level of comminuted host rock. The fault walls are characterized by pre-existing fractures which consist of parallel and discrete fractures (FS_1), with regular spacing (up to 8 fractures per meter, Fig. 11b) and at high angles (72° on average) to the fault plane (Fig. 15). Their orientation (N140°-150°) is consistent with FS_1 fractures, as reconstructed in the whole Calcione area (Figs. 5 and 6). Nevertheless, FS_2 fractures giving rise

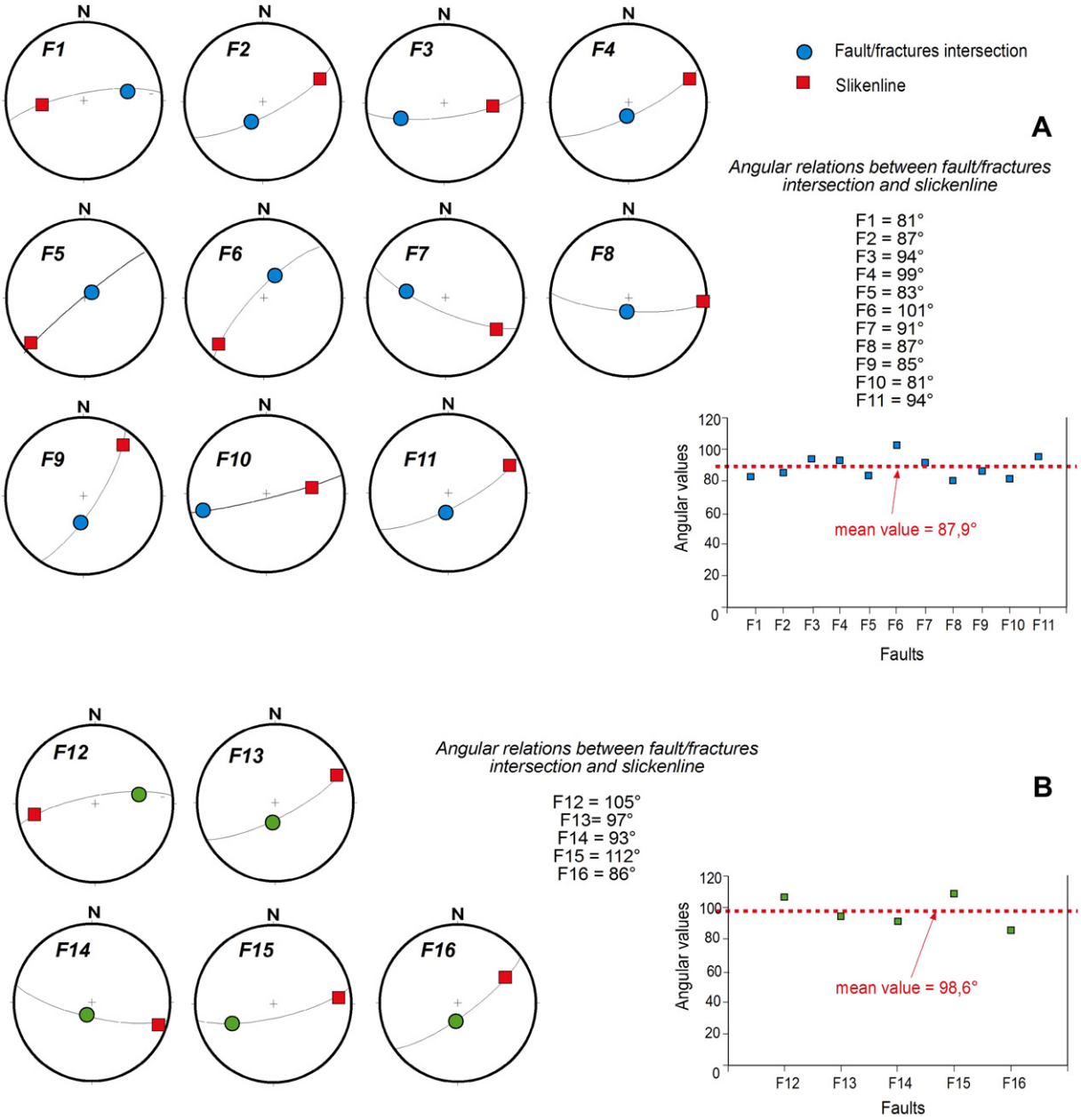

Fig. 13. Stereographic diagrams (Schmidt diagram, lower hemisphere) showing the slickenline and the fault/fracture intersections for each analyzed fault. The fault/fracture intersection derives from the interaction of fault plane and fifteen fractures. The angular values have been also reported.

to clustering within rock lithons defined by FS_1 structures are also present. In some cases, FS_2 fractures show a parallel trend with respect to the strike-slip faults.

The kinematics of the fault has been defined by calcite slickenfibers with lunate structures and slickensides on the polished fault plane, suggesting left-lateral strike-slip movement (Fig. 15a–b). Relationships between fault length (fl) and maximum fracture length (mfl) are reported in Fig. 12a. These scaling relationships do not fit the other cases described in the previous paragraph or data from the literature. This is discussed in the next paragraph.

Fig. 16 illustrates a similar case but highlights differences for the damage zone fracture network. The fault core is mainly represented by millimeter-thick gouges derived from comminution of the wall rock. Millimeter and sub-millimeter calcite veins, composed of aligned crystal fibers, grew on the slip plane showing a N80° trend striking. Calcite fiber growth and mechanical striations indicate a main horizontal displacement with left-lateral movement. The fault affected fractured sandstone characterized by pre-existing fractures, mainly N140°–150° striking and consistent with FS_1 fractures. As described for the previous case, FS_2 fractures also developed in lithons defined by the main FS_1 fractures. FS_1 fractures are regularly spaced (up to 5 fractures per meter) and dissected at a high angle (75° on average) by the fault. Other shorter fractures developed at low angles to the fault plane, mainly in the southern wall at 15–35° to the fault plane. Low angle fractures have en-échelon distribution and are parallel and discrete with a spacing up to 15 fractures per meter. The resulting fracture network is asymmetric: the northern wall is characterized by (pre-existing) fractures at high angles to the fault plane; the southern wall shows fractures at high and low angles to the fault plane (Fig. 16). The relationships between fault length (fl) and maximum fracture length (mfl) is reported in Fig. 12a for the different fracture sets.

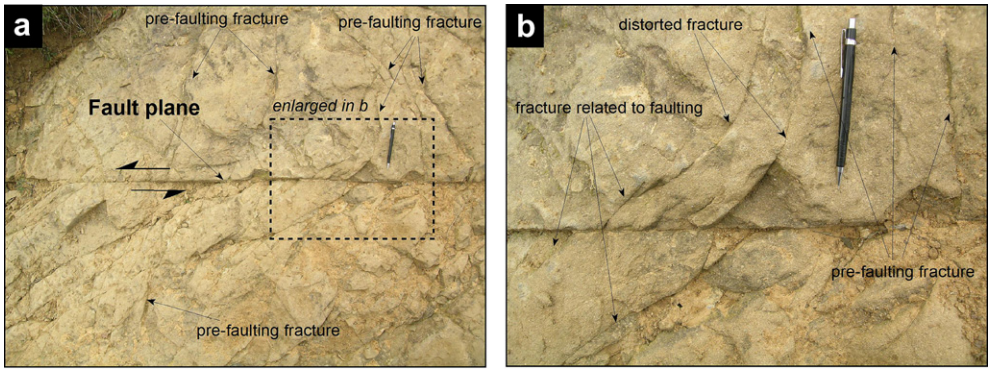

Fig. 14. Photographs illustrating a curvilinear fracture developed in a fault damage zone. Its curvilinear plane is due to the interference of the newly-formed fracture with a pre-existing one (see the text for more details).

Scaling relationships from low angle fractures fit the cases described in the previous paragraph and data from the literature, whereas those from high angle fractures are anomalous (Fig. 12a).

Fig. 17 illustrates the selected case of strike-slip faults superimposed obliquely on pre-existing fractures. The fault core consists of millimeter-thick gouges. Calcite fiber growth coupled with mechanical striations on the fault plane indicate a main horizontal displacement with left-lateral movement. Here a left-lateral strike-slip fault, oriented N110°, dissected sandstone with pre-existing FS_1 and FS_2 fractures, striking about N140–150° and N70–120°, respectively. The fracture pattern in the damage zone is a herring-bone network (Fig. 17); this geometrical configuration is derived from superimposition of fractures associated with faulting on pre-existing fractures. Fractures intersect the main fault plane at low angles (25–50°) in both fault walls, and are characterized by similar spacing and length, despite slightly different intersecting angular values in the two fault walls (Fig. 17). The relationships between fault length (fl) and maximum fracture length (mfl) do not fit the scaling relation of Fig. 12a.

Angular relations between the fault/fracture intersection and fault slickenlines (cf. Blenkinsop, 2008) are also illustrated in Fig. 13B and discussed in the next paragraph.

5. Discussion

In the last few decades, much research has been dedicated to the architecture of strike-slip faults over a wide range of magnitude of fault displacements. It has been demonstrated that strike-slip faults of very different sizes in different rocks show comparable geometrical patterns in terms of fracture network and scaling relationships,

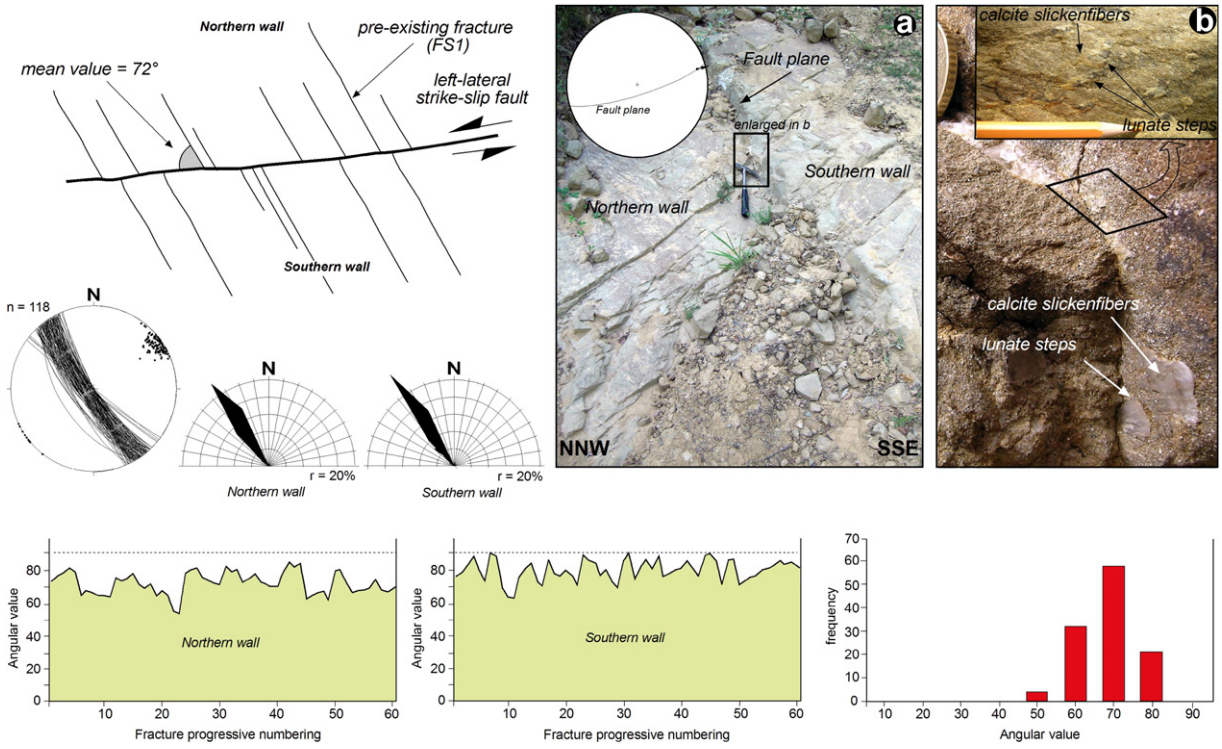

Fig. 15. Fault/fractures angular relationships simulating a right-lateral movement, opposite with respect to the true kinematics. Fractures intersecting the fault plane predate the development of fault. Stereographic diagram (lower hemisphere, Schmidt diagram) illustrates the great circles of the fractures and related poles; the rose diagrams show fractures measured in the indicated fault walls. The histograms indicate, from the left: the angular values at the intersection between the fault plane and the fractures occurring in the indicated fault walls; the cumulative angular values measured at the intersection between the fault plane and the fractures in the fault walls.

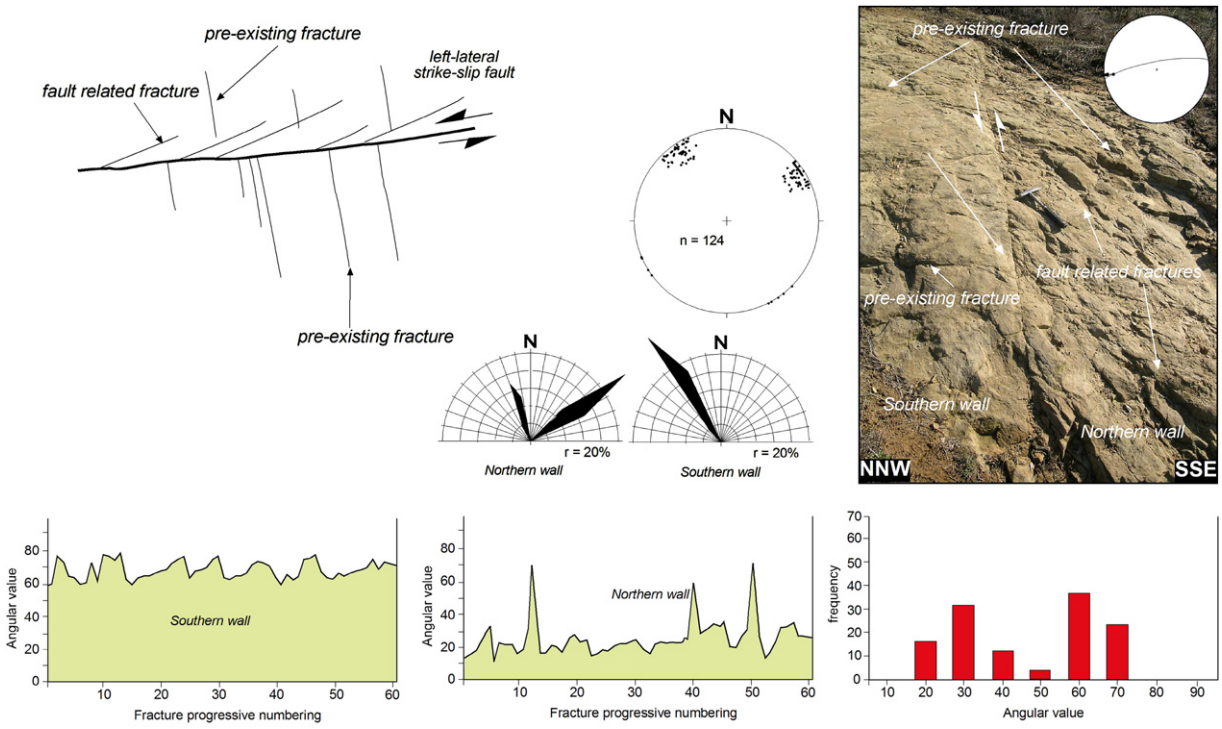

Fig. 16. Two fracture sets intersecting the fault plane (see the text for more information); the fractures at low angle to fault plane consist of synthetic fractures developed during faulting. Fractures at high angles to fault plane consist of pre-existing fractures. The fracture pattern is ambiguous: the fault/fractures intersection simulating a right-lateral movement is opposite with respect to the true kinematics. The stereographic diagram (lower hemisphere, Schmidt diagram) illustrates poles of the fractures; the rose diagrams show fractures measured in the indicated fault walls. The diagrams show, from the left: the measured angular values at the intersection between the main fault plane and the main fractures in the indicated fault walls; the cumulative angular values measured at the intersection between the fault plane and the fractures in the fault walls.

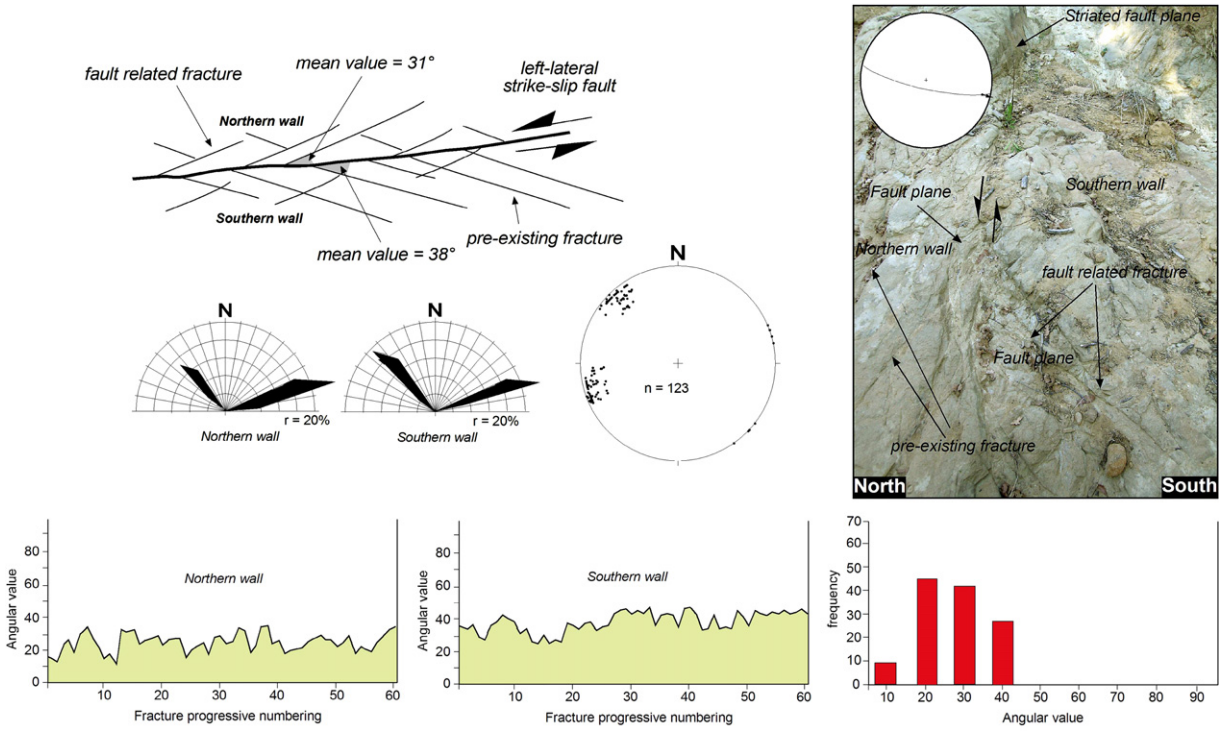

Fig. 17. Herringbone-shape fractures characterizing strike-slip fault damage zones. These fracture pattern derives from two intersecting fracture sets. One fracture set consists of pre-existing fractures on which neoformational ones, related to faulting, superimposed.

combining different parameters: i) length of fault segments, ii) length of fractures (splay) forming damage zones; iii) displacement, iii) length of overstepping relay zones, iv) width of overstepping relay zones. Negative and positive power law relationships have been demonstrated between these different geometrical elements: fault segment length *vs* fracture length (de Joisseneau and Aydin, 2007), fracture length *vs* offset (Wesnousky, 1988; Sieh and Natawidjaja, 2000; Jachens et al., 2002; Walker and Jackson, 2002; Tatar et al., 2004; Fu and Awata, 2006; Nemer and Meghraoui, 2006; Rovida and Tibaldi, 2005; de Joisseneau et al., 2007; de Joisseneau and Aydin, 2009), width of damage zone *vs* offset, length of fault *vs* offset (Cowie and Scholz, 1992); maximum offset *vs* step width and maximum offset *vs* step length (Wesnousky, 1988; Stirling et al., 1996; Sieh and Natawidjaja, 2000; Le Pichon et al., 2001; Jachens et al., 2002; Maruyama and Lin, 2002; Walker and Jackson, 2002; Tatar et al., 2004; Fu and Awata, 2006; Nemer and Meghraoui, 2006; de Joisseneau and Aydin, 2009); step length *vs* step width (Aydin and Nur, 1982; Wesnousky, 1988; Stirling et al., 1996; Sieh and Natawidjaja, 2000; Le Pichon et al., 2001; Jachens et al., 2002; Maruyama and Lin, 2002; Walker and Jackson, 2002; Tatar et al., 2004; Nemer and Meghraoui, 2006; Fu and Awata, 2006; de Joisseneau and Aydin, 2009); maximum fault offset *vs* steps per km (Wesnousky, 1988; Lawrence et al., 1992; Stirling et al., 1996; Sieh and Natawidjaja, 2000; Langenheim et al., 2001; Le Pichon et al., 2001; Jachens et al., 2002; Walker and Jackson, 2002; Maruyama and Lin, 2002; Pachell and Evans, 2002; Brankman and Aydin, 2004; Rhodes et al., 2004; Tatar et al., 2004; Cembrano et al., 2005; Rovida and Tibaldi, 2005; Nemer and Meghraoui, 2006; Fu and Awata, 2006; Walker et al., 2006; de Joisseneau and Aydin, 2009).

In the study area, relations between the different geometrical parameters of faults not interfering with pre-existing fractures (Figs. 9 and 12) agreed with the scaling relations highlighted by other workers. In particular, data on the relation between mean step length and mean step width in overstepping fault segments fit the positive power law as reconstructed by de Joisseneau and Aydin (2009) and references therein. The relation between fault length and maximum fracture length (Fig. 12a) also fit the positive power law as highlighted in other areas by de Joussineau et al. (2007). However, no differences in angular values between faults and their fractures (splay angle in Aydin and Berryman, in press) were recognized for different fault configurations (i.e. isolated fault segments and interacting fault segments), in contrast with the observation of de Joisseneau and Aydin (2007) for the Valley of Fire State Park (Nevada, USA). I observed angular values ranging from 20° to 50° (Fig. 10) for isolated and interacting fault segments (Fig. 9). In contrast, I observed different angular values in wall and tip damage zones with means ranging from 20° to 42° and 35°–50°, respectively. Although splay angles depend on different factors mainly related to the nature of the affected lithotypes (Fletcher and Pollard, 1981; Hancock, 1985; Willemse and Pollard, 1998; Pollard and Aydin, 1988; Martel, 1990; Cruikshank and Aydin, 1994; Cooke, 1997; Younes and Engelder, 1999; Mollema and Antonellini, 1999; Peacock, 2001; Kim et al., 2004), the different angles in wall and tip damage zones are probably due to different mechanical responses to deformation.

Irrespective of angular values, it is accepted that fault/fracture angular relationships are useful indicators for reconstructing the lateral sense of movement of strike-slip faults (Kim et al., 2004 for a review). On the other hand, temporal relationships between fractures and faults have important geological implications for the kinematics of faults and the tectonic history of a region (Peacock, 2001 and references therein). In fact, various papers describe pre-existing fractures influencing fault development in terms of geometrical configuration (Martel et al., 1988; Martel, 1990, 1999; Peacock and Sanderson, 1992; Myers and Aydin, 2004; Flodin and Aydin, 2004; Van Der Zee et al., 2008). Myers and Aydin (2004) and Flodin and Aydin (2004), studying Jurassic sandstones exposed in the Valley of Fire, State Park (southern Nevada, USA), recently documented the effect of superimposed strike-slip faults in rock masses affected by pre-existing fractures. Flodin and Aydin (2004) documented anomalous splay angles, as new generations of faults and fractures formed along pre-existing joints (Myers and Aydin, 2004). Thus, pre-existing or precursor structures such as joints, veins or solution surfaces and deformation bands can influence the geometry of splays, explaining certain outstanding issues of fault zone complexity (Crider and Peacock, 2004 with references therein). For example, Cruikshank et al. (1991) and Myers and Aydin (2004) described faults along pre-existing joints linked by wing cracks in sandstone. Summing up, previous work demonstrates that pre-existing fractures in rock masses later

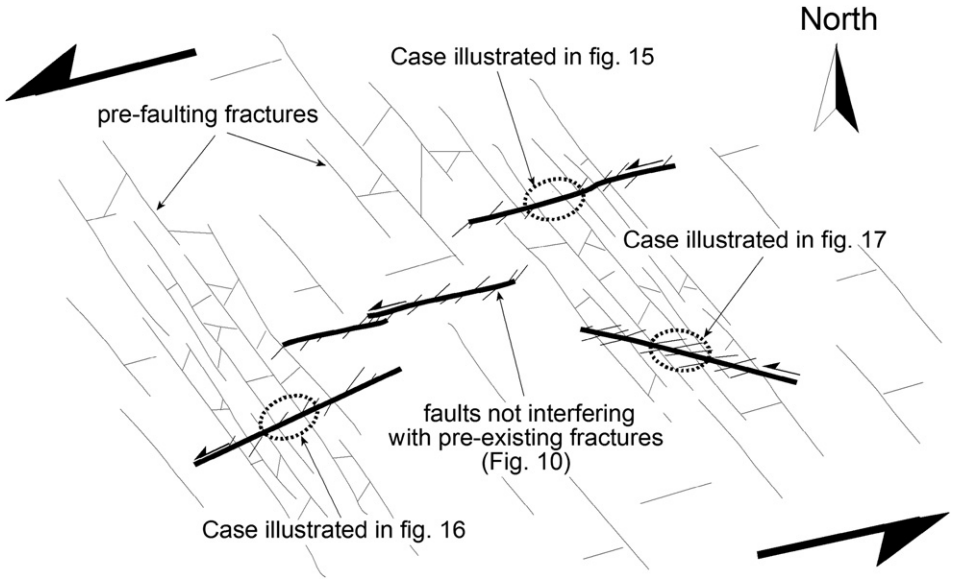

Fig. 18. Cartoon illustrating the conceptual model dealing with the relationships between strike-slip faults and pre-existing fractures. Intersection at different angles gave rise to different geometric configurations of fractures. The different cases illustrated in the text are also indicated.

affected by strike-slip faults may produce local fault/fracture angular relationships indicating a lateral sense of movement opposite to the true one. Some strike-slip faults described for the Calcione area strengthen Flodin and Aydin's concept and provide another example illustrating how pre-existing fractures in sandstone can influence the fault growth process, giving rise to anomalous fracture/fault angular relationships. Different fracture patterns developed in damage zones (Figs. 14–17) and depended on intersecting angular values between the pre-existing fractures and the strike-slip faults (Fig. 18).

Most strike-slip faults developed at high angles to the pre-existing fractures (Fig. 18). In such cases, pre-existing discrete, parallel and regularly spaced discontinuities (Figs. 5 and 6) could inhibit the formation of splay during faulting, leading to anomalous fracture patterns. Failure to recognize kinematic indicators on the fault plane may result in deception. For example, the case illustrated in Fig. 15 highlights a left-lateral strike-slip fault characterized by decimeter offset; the acute angles suggest right-lateral movement, which is opposite to the true sense of movement, as indicated by the kinematic indicators on the fault plane. Newly-formed fractures associated with strike-slip faulting are lacking, probably due to the embryonic stage of fault growth (cf. de Joissineau et al., 2007) or, alternatively, due to the fact that the forces defining the principal stress components acting on the fault plane dissipated with reactivation of the pre-existing fractures, which performed as shear fractures. In this case, they should have sheared in a right-lateral sense due to the complementary shear stress. Possible shearing along pre-existing fractures cannot be defined and the acute angles (72° in Fig. 15) are inconsistent with those measured for splays related to strike-slip faults in sandstone not affected (or relatively unaffected) by pre-existing fractures (Fig. 10) or described in the literature (de Joisseneau and Aydin, 2007; de Joisseneau and Aydin, 2009), which range from 15° to 50°. Also, the relationships between fault length and maximum fracture length do not fit those documented by other researchers (Fig. 12a). Thus, angular values and geometrical relationships between fault segment length and fracture length can be considered useful for discriminating deceptive cases.

Strike-slip faults developing at low angles to pre-existing fractures gave rise to a very ambiguous fracture pattern (Fig. 17). The overall real lateral sense of movement cannot be defined with certainty if only a part of the fault damage zone is exposed. However, to discriminate pre-existing from newly-formed fractures, useful insights can be obtained from cross-cutting and abutting relationships (Segall and Pollard, 1983; Cruikshank et al., 1991; Wilkins et al., 2001). Indeed, pre-faulting fractures (mode I opening fractures) should be preserved in lithons delimited by newly-formed structures, and if so, they were not reactivated. In the study area, pre-existing fractures with no shear provide circumstantial evidence that most of these structures were not reactivated. This is conceptually sound evidence but reactivation of pre-existing fractures is a real possibility that cannot be excluded, as demonstrated by Flodin and Aydin (2004). In fact, it is unlikely that deformation would create strike-slip faults at a very low angle to a pre-existing fracture system instead of taking advantage of the fracture system. In this view, FS_2 fractures probably favored development of the strike-slip faults, since they are roughly parallel to the strike of the faults (see Fig. 18).

The analyses of angular relations between fault/fracture intersection and slickenline offer another stimulating consideration: in most cases the slip direction lies perpendicular to the line defined by the fault/fracture intersection, as illustrated in Fig. 3b and c. In the study area this geometrical relation has been documented for all faults not interfering with pre-existing structures (Fig. 13A), where a mean angular value of 87.9° has been calculated. On the contrary, 98.6° is the mean angular value obtained from the fault/fracture intersection and slickenline for strike-slip faults dissecting rock masses affected by pre-existing fractures (Fig. 13B). Fig. 13B shows field examples of oblique relationships between fault/fracture intersection lines and related fault slip vectors. This anomalous geometrical relation could be related to pre-existing fractures that influenced the final geometric configuration of fractures in the damage zones of the newly-formed strike-slip faults (cf. Blenkinsop, 2008).

6. Conclusion

Analysis of strike-slip faults in sandstone exposed in the Calcione area highlighted the critical role of pre-existing fractures in the development of these faults and configuration of their damage zones. New data for the architecture of strike-slip fault systems is provided for faults dissecting rock masses not affected by pre-existing fractures. The new data set lends support to previously published data on general trends in fault scaling. In particular: i) the scaling relation between fault length and maximum fracture length in the damage zone agreed with the positive power law reconstructed for other sites around the world; ii) the scaling relation between the mean length and mean width of steps in overstepping fault segments was in line with the positive power law defined by other authors; iii) the little available data on the relation between mean length and width of steps of understepping fault segments followed a positive power law trend.

The relation between fault length and maximum fracture lengths of faults dissecting sandstone affected by pre-existing fractures does not show scaling relations. Variations in fracture patterns in damage zones provides ambiguous cases that could lead to incorrect evaluation of faults kinematics. The angular relationships between pre-existing fractures and the fault plane may simulate splays apparently related to faulting. This is a critical point for tectonic investigation because fault kinematics can be misinterpreted. However, four main points are defined for detecting deceptive cases in study areas. There is a real probability of a deceptive fracture pattern if: i) angular values at the intersection of the fault and its fractures (mode I opening fracture) exceed 50° in the wall damage zone; ii) the scaling relation between fault length and maximum fracture length does not fit the power law reported in Fig. 12a; iii) the angular relation between fault/fracture line and slip vector is different from 90°; iv) fractures acted as shear fractures. The fourth point could prove unreliable.

In any case, accurate description of protolith fabric and reconstruction of the pre-faulting structural setting are fundamental for understanding anomalous fracture patterns in fault damage zones. Particular care is therefore needed when strike-slip faults dissected rock masses affected by pre-existing fractures, especially if the faults developed at high angles to the fractures. In such cases, reconstructions of fault kinematics can be flawed by erroneous interpretations.

Acknowledgements

I wish to thank Atilla Aydin and Thomas Blenkinsop for the fruitful suggestions, comments and criticisms which helped me to improve the quality of data and manuscript text. R.E. Holdsworth is also thanked for the editorial support and assistance. Thanks to S. Jones for the English revision.

References

Abou Elenean, K.M., Mohamed, A.M.E., Hussein, H.M., 2010. Source parameters and ground motion of the Suez-Cairo shear zone earthquakes, Eastern Desert, Egypt. Nat. Hazards 522, 431–451.

Acocella, V., Funiciello, R., 2005. Transverse systems along the extensional Tyrrhenian margin of central Italy and their influence on volcanism. Tectonics 25. doi:10.1029/2005TC00184.
Adiyaman, Ö, Chorowicz, J., 2002. Late Cenozoic tectonics and volcanism in the northwestern corner of the Arabian plate: a consequence of the strike-slip Dead Sea fault zone and the lateral escape of Anatolia. J. Volc. Geoth. Res. 117, 327–345.
Agosta, F., Aydin, A., 2006. Architecture and deformation mechanism of a basin-bounding normal fault in Mesozoic platform carbonates, central Italy. J. Struct. Geol. 28, 1445–1467.
Albarello, D., Batini, F., Bianciardi, P., Ciulli, B., Spinelli, E., Viti, M., 2005. Stress field assessment from ill-defined fault plane solutions: an example from the Larderello Geothermal Field (western Tuscany, Italy). Boll. Soc. Geol. It. Spec 3, 187–193.
Aldinucci, M., Ghinassi, M., Sandrelli, F., 2007. Climatic and tectonic signature in the fluvial infill of a late Pliocene Valley (Siena basin, northern Apennines, Italy). J. Sed. Res. 77, 398–414.
Aqué, R., Brogi, A., 2002. La dorsale Monti del Chianti-Monte Cetona nel quadro evolutivo della Catena appenninica settentrionale: tettonica polifasata nella trasversale Trequanda-Sinalunga (Toscana meridionale). Boll. Soc. Geol. It. 121, 365–376.
Aydin, A., 1978. Small faults formed as deformation bands in sandstone. Pure Appl. Geophys. 116, 913–930.
Aydin, A., 2000. Fractures, faults, and hydrocarbon entrapment, migration and flow. Marine Petrol. Geol. 17, 797–814.
Aydin, A., Berryman J.G. Analysis of the growth of strike-slip faults using effective medium theory. J. Struct. Geol., in press, doi:10.1016/jsg.2009.11.007.
Aydin, A., Johnson, A., 1978. Development of faults as zones of deformation bands and as slip surfaces in sandstone. Pure Appl. Geophys. 116, 931–942.
Aydin, A., Johnson, A.M., 1983. Analysis of faulting in porous sandstones. J. Struct. Geol. 5, 19–31.
Aydin, A., Nur, A., 1982. Evolution of pull-apart basins and their scale independence. Tectonics 1, 91–105.
Bartlett, W.L., Friedman, M., Logan, J.M., 1981. Experimental folding and faulting in rocks under confining pressure, part IX: wrenck faults in limestone layers. Tectonics 79, 255–277.
Bastesen, E., Braathen, A., Henning, H., Gabrielsen, R.H., Skar, T., 2009. Extensional fault cores in micritic carbonate. Case studies from the Gulf of Corinth, Greece. J. Struct. Geol. 31, 403–420.
Bellot, J.P., 2008. Hydrothermal fluids assisted crustal-scale strike-slip on the Argentat fault zone. Tectonophysics 450, 21–33.
Berg, S.S., Skar, T., 2005. Controls on damage zone asymmetry of a normal fault zone: outrcrop analysis of a segment of the Moab fault, SE Utah. J. Struct. Geol. 27, 1803–1822.
Biddle, K.T., Christie-Blick, N., 1985. Strike-slip Deformation, Basin Formation, and Sedimentation. In: Soc. Econ. Paleont. Min. Spec. Publ., 37.
Billi, A., Salvini, F., Storti, F., 2003. The damage zone – fault core transition in carbonate rocks: implications for fault growth, structure and permeability. J. Struct. Geol. 25, 1779–1794.
Blenkinsop, T.G., 2008. Relationships between faults, extension fractures and veins, and stress. J. Struct. Geol. 30, 622–632.
Bonini, M., 1999. Basement-controlled Neogene polypshase cover thrusting and basin development along the Chianti Mountains ridge (Northern Apennines, Italy). Geol. Mag 136, 133–152.
Bonini, M., Sani, F., 2002. Extension and compression in the northern Apennines (Italy) hinterland: evidence from the late Miocene–Pliocene Siena-Radicofani Basin and relations with basement structures. Tectonics 22, 1–35.
Bossio, A., Costantini, A., Lazzarotto, A., Liotta, D., Mazzanti, R., Mazzei, R., Salvatorini, G.F., Sandrelli, F., 1993. Rassegna delle conoscenze sulla stratigrafia del Neoautoctono toscano. Mem. Soc. Geol. It 49, 17–98.
Brankman, C.M., Aydin, A., 2004. Uplift and contractional deformation along a segmented strike-slip fault system: the Gargano Promontory, southern Italy. J. Struct. Geol. 26, 807–824.
Brogi, A., 2004. Faults linkage, damage rocks and hydrothermal fluid circulation: tectonic interpretation of the Rapolano Terme travertines (southern Tuscany, Italy) in the context of Northern Apennines Neogene-Quaternary extension. Eglog. Geol. Helv 97, 307–320.
Brogi, A., 2008. Fault zone architecture and permeability features in siliceous sedimentary rocks: insights from the Rapolano geothermal area (Northern Apennines, Italy). J. Struct. Geol. 30, 237–256.
Brogi, A., Capezzuoli, E., 2009. Travertine deposition and faulting: the fault-related travertine fissure-ridge at Terme S. Giovanni, Rapolano Terme (Italy). Int. J. Earth Sci. (Geol. Rundsch.) 98, 931–947. doi:10.1007/s00531-007-0290-z.
Brogi, A., Capezzuoli, E., Aqué, R., Branca, M., Voltaggio, M., 2009. Studying travertines for neotectonics investigations: Middle–Late Pleistocene syn-tectonic travertine deposition at Serre di Rapolano (Northern Apennines, Italy). Int. J. Earth Sci. (Geol. Rundsch.). doi:10.1007/s00531-009-0456-y.
Brogi, A., Costantini, A., Lazzarotto, A., 2002. Tectonic setting of the Rapolano-Trequanda ridge. Boll. Soc. Geol. It. Spec. 1, 757–768.
Brogi, A., Lazzarotto, A., Liotta, D., CROP18 Working Group, 2005. Structural features of southern Tuscany and geological interpretation of the CROP18 seismic reflection survey (Italy). Boll. Soc. Geol. It. Spec. 3, 213–236.
Brogi, A., Liotta, D., 2008. Highly extended terrains, lateral segmentation of the substratum, and basin development: the Middle–Late Miocene Radicondoli Basin (inner Northern Apennines, Italy). Tectonics 27. doi:10.1029/2007/TC002188 TC5002.
Brogi, A., Liotta, D., Meccheri, M., Fabbrini, L., 2010. Transtensional shear zones controlling volcanic eruptions: the Middle Pleistocene Mt. Amiata volcano (inner Northern Apennines, Italy). Terra Nova 22, 137–146.
Caine, S.J., Evans, J.P., Forster, C.B., 1996. Fault zone architecture and permeability structure. Geology 24, 1025–1028.
Cakir, M., Aydin, A., Campagna, D.J., 1998. Deformation pattern around conjoining strike-slip faults systems in the Basin and Range, southeast Nevada: the role of strike-slip faulting in basin formation and inversion. Tectonics 17, 344–359.
Carmignani, L., Decandia, F.A., Disperati, L., Fantozzi, P.L., Kligfield, R., Lazzarotto, A., Liotta, D., Meccheri, M., 2001. Inner Northern Apennines. In: Vai, G.B., Martini, I.P. (Eds.), Anatomy of an Orogen: The Apennines and Adjacent Mediterranean Basins. Kluwer Academic, Dordrecht.
Carmignani, L., Decandia, F.A., Disperati, L., Fantozzi, P.L., Lazzarotto, A., Liotta, D., Meccheri, M., 1994. Tertiary extensional tectonics in Tuscany (Northern Apennines Italy). Tectonophysics 238, 295–315.
Carmignani, L., Lazzarotto, A., 2004. Carta Geologica Della Toscana Alla Scala 1:250.000. Selca, Firenze.
Catchings, R.D., Rymer, M.J., Goldman, M.R., Gandhok, G., 2009. San Andreas fault geometry at Desert Hot springs, California, and its effects on earthquake hazards and Groundwater. Bull. Seism. Soc. Am. 99, 2190–2207.
Cembrano, J., González, G., Arancibia, G., Ahumada, I., Olivares, V., Herrera, V., 2005. Fault zone development and strain partitioning in an extensional strike-slip duplex: a case study from the Mesozoic Atacama fault system, Northern Chile. Tectonophysics 400, 105–125.
Chester, F.M., Evans, J.P., Biegel, R.L., 1993. Internal structure and weakening mechanism of the *S. Andreas* Fault. J. Geoph. Res. 98, 771–786.
Chester, F.M., Logan, J.M., 1986. Implications for mechanical properties of brittle faults from observations of the Punchbowl fault zone, California. Pure Appl. Geophys. 124, 79–106.
Cipriani, N., Ercoli, A., Malesani, P., Vannucci, S., 1972. I travertini di Rapolano Terme (Siena). Mem. Soc. Geol. It. 11, 31–46.
Cloos, H., 1928. Experiment zur inneren Tektonik. Centralblatt fur Mineralogie and Paleontologie 1928B, 609.
Cooke, M.L., 1997. Fracture localization along faults with spatially varying friction. J. Geoph. Res. 102, 22425–22434.
Cornamusini, G., 2002. Compositional evolution of the Macigno Fm. of southern Tuscany along a transect from the Tuscan coast to the Chianti Hills. Boll. Soc. Geol. It. Spec. Vol. 1, 365–374.
Corti, G., Carminati, E., Mazzarini, F., Garcia, M.O., 2005. Active strike-slip faulting in El Salvador, central America. Geology 33, 989–992.
Costantini, A., Lazzarotto, A., Sandrelli, F., 1982. Conoscenze geologico strutturali. In: il Graben di Siena. CNR PFE RF9, 11–32.
Cowie, P.A., Scholz, C.H., 1992. Physical explanation for the displacement-lenght relationships of faults usind a post-yield fracture mechanics model. J. Struct. Geol. 14, 1133–1148.
Crider, J.G., Peacock, D.C.P., 2004. Initiation of brittle faults in the upper crust: a review of field observations. J. Struct. Geol. 26, 691–707.
Cruikshank, K.M., Aydin, A., 1994. Role of fracture localization in arch formation, Arches National Park. Utah Geol. Soc. Am. Bull. 106, 879–891.
Cruikshank, K.M., Zhao, G., Johnson, A.M., 1991. Analysis of minor fractures associated with joints and faulted joints. J. Struct. Geol. 13, 865–886.
Davis, G.H., Bump, A.P., Garcìa, P.E., Ahlgren, S.G., 2000. Conjugate Riedel deformation band shear zones. J. Struct. Geol. 22, 169–190.
Davatzes, N.C., Aydin, A., 2003. Overprinting faulting mechanisms in sanstone. J. Struct. Geol. 25, 1795–1813.
Devatzes, N.C., Aydin, A., Eichhubl, P., 2003. Overprinting faulting mechanism during the development of multiple fault sets in sandstone, Chimney Rock, Utah. Tectonophysics 363, 1–18.
de Joisseneau, G., Aydin, A., 2007. The evolution of the damage zone with fault growth in sandstone and its multiscale characteristics. J. Geoph. Res. 112. doi:10-1029/2006JB004711 B 12401.
De Joussineau, G., Mutlu, O., Aydin, A., Pollard, D.D., 2007. Characterization of strike-slip fault-splay relationships in sandstone. J. Struct. Geol. 29, 1831–1842.
de Joisseneau, G., Aydin, A., 2009. Segmentation along strike-slip faults revisited. Pure Appl. Geophys. 166, 1575–1594.
de Ronde, C.E.J., Sibson, R.H., Bray, C.J., Faure, K., 2001. Fluid chemistry of veining associated with an ancient microearthquake swarm, Benmore Dam. New Zealand. Bull. Geol. Soc. Am. 113, 1010–1024.
Delacou, B., Deichmann, N., Sue, C., Thouvenot, F., Champagnac, J.D., Burkhard, M., 2005. Active strike-slip faulting in the Chablais area (NW Alps) from earthquake focal mechanisms and relative locations. Eclogae Geol. Helv. 98, 189–199.
Della Vedova, B., Bellani, S., Pellis, G., Squarci, P., 2001. Deep temperatures and surface heat £ ow distribution. In: Vai, G.B., Martini, I.P. (Eds.), Anatomy of an Orogen: The Apennines and Adjacent Mediterranean Basins. Kluwer Academic Publishers, Amsterdam, pp. 65–76.
Dini, A., Gianelli, G., Puxeddu, M., Ruggieri, G., 2005. Origin and evolution of Pliocene-Pleistocene granites from the Larderello geothermal field (Tuscan magmatic Province, Italy). Lithos. 81, 1–31.
Dini, A., Innocenti, F., Rocchi, S., Tonarini, S., Westerman, D.S., 2002. The magmatic evolution of the late Miocene laccolith–pluton–dyke granitic complex of Elba Island. Italy. Geol. Mag. 139, 257–279.
Dini, A., Mazzarini, F., Musumeci, G., Rocchi, S., 2008. Multiple hydro-fracturing by boron-rich fluids in the Late Miocene contact aureole of Eastern Elba Island (Tuscany, Italy). Terra Nova 20, 318–326.

Dong, Y.x., Wang, Z.c., Zheng, H.j., Xu, A.n, 2008. Control of strike-slip faulting on reservoir formation of oil and gas in Nanpu sag. Pet. Exploration Dev. 35, 424–430.
Drukpa, D., Velasco, A.A., Doser, D.I., 2006. Seismicity in the Kingdom of Bhutan (1937-2003): evidence for crustal transcurrent deformation. J. Geoph. Res. Solid Earth 111, b06301.
Elter, F.M., Sandrelli, F., 1994. La fase post-nappe nella Toscana meridionale: nuova interpretazione sull'evoluzione dell'Appennino Settentrionale. Atti. Ticinesi. di. Scienze. della. Terra. 37, 173–193.
Etiope, G., Guerra, M., Raschi, A., 2005. Carbon dioxide and radon geo-hazards over a gas-bearing fault in the Siena Graben (Central Italy). Terr. Atm. Ocean. Sci. 16, 885–896.
Fletcher, R.C., Pollard, D.D., 1981. Anticrack model for pressure solution surfaces. Geology 9, 419–424.
Flodin, E., Aydin, A., 2004. Faults with asymmetric damage zones in sandstone, Valley of Fire State Park, southern Nevada. J. Struct. Geol. 26, 983–988.
Fu, B., Awata, Y., 2006. Displacement and timing of left-lateral faulting in the Kunlun Fault Zone, northern Tibet, inferred from geologic and geomorphic features. J. Asian Earth Sci. 29, 253–265.
Garcìa-Palomo, A., Macìas, J.L., Espìndola, J.M., 2004. Strike-slip faults and K-alkaline volcanism at El Chichón volcano, southeastern Mexico. J. Volc. Geoth. Res. 136, 247–268.
Hancock, P.L., 1985. Brittle microtectonics: principles and practice. J. Struct. Geol. 7, 437–457.
Harris, R.A., Archuleta, R.J., Day, S.M., 1991. Fault steps and the dynamic rupture process: 2-d simulation of a spontaneously propagating shear fractures. Geophys. Res. Lett. 18, 893–896.
Healy, D., Jones, R.R., Holdsworth, R.E., 2006. Three-dimensional brittle shear fracturing by tensile crack interaction. Nature 439, 64–67.
Jachens, R.C., Langenheim, V.E., Matti, J.C., 2002. Relationship of the 1999 Hector Mine and 1992 Landers fault ruptures to offsets on Neogene faults and distribution of late Cenozoic basins in the eastern California shear zone. Bull. Seismol. Soc. Am. 92, 1592–1605.
Kelly, P.G., Sanderson, D.J., Peacock, D.C.P., 1998. Linkage and evolution of conjugate strike-slip fault zones in limestone of Somerset and Northumbria. J. Struct. Geol. 20, 1477–1493.
Kim, Y.S., Peacock, D.C.P., Sanderson, D.J., 2003. Mesoscale strike-slip faults and damage zones at Marsalforn, Gozo Island, Malta. J. Struct. Geol. 25, 793–812.
Kim, Y.S., Peacock, D.C.P., Sanderson, D.J., 2004. Fault damage zones. J. Struct. Geol. 26, 503–517.
Langenheim, V.E., Grow, J.A., Jachens, R.C., Dixon, G.L., Miller, J.J., 2001. Geophysical constraints on the location and geometry of the Las Vegas Valley shear zone, Nevada. Tectonics 20, 189–209.
Lawrence, R.D., Hasan Khan, S., Nakata, T., 1992. Chaman fault, Pakistan-Afghanistan. Ann. Tectonicae 6, 196–223.
Lazar, M., Ben-Avraham, Z., Schattner, U., 2006. Formation of sequential basins along a strike–slip fault–Geophysical observations from the Dead Sea basin. Tectonophysics 421, 53–69.
Lazzarotto, A., 1973. Caratteri strutturali dei nuclei mesozoici di Montalceto, Trequanda e Piazza di Siena (Prov. di Siena). Atti Soc. Tosc. Sc. Nat. Mem. Serie A 79, 251–266.
Le Pichon, X., Sengor, A.M.C., Demirbag, E., Rangin, C., Imren, C., Armijo, R., Gorur, N., Cagatay, N., Mercier De Lepinay, B., Meyer, B., Saatcilar, R., Tok, B., 2001. The active main Marmara fault. Earth Planet. Sci. Lett. 192, 595–616.
Liotta, D., 1996. Analisi del settore centro-meridionale del bacino pliocenico di Radicofani (Toscana meridionale). Boll. Soc. Geol. It. 115, 115–143.
Liotta, D., Cernobori, L., Nicolich, R., 1998. Restricted rifting and its coexistence with compressional structures: results from the Crop03 traverse (Northern Apennines Italy). Terra Nova 10, 16–20.
Losacco, U., Del Giudice, D., 1958. Stratigrafia e tettonica degli affioramenti mesozoici posti fra le colline di Rapolano ed il Monte Cetona (Siena). Boll. Soc. Geol. It. 77, 1–32.
Mann, P., Hempton, M.R., Bradley, D.C., Burke, K., 1983. Development of pull-apart basins. J. Geol. 91, 529–554.
Martel, S.J., 1999. Mechanical controls on fault geometry. J. Struct. Geol. 21, 585–596.
Martel, S.J., 1990. Formation of compound strike-slip fault zones, Mount Abbot Quadrangle, California. J. Struct. Geol. 12, 869–882.
Martel, S.J., Pollard, D.D., Segall, P., 1988. Development of simple strike-slip fault zones, Mount Abbot quadrangle, Sierra Nevada, California. Geol. Soc. Am. Bull. 100, 1451–1465.
Martini, I.P., Sagri, M., 1993. Tectono-sedimentary characteristics of the late Miocene-Quaternary extensional basins of the Northern Apennines, Italy. Earth Sci. Rev. 34, 197–233.
Maruyama, T., Lin, A., 2002. Active strike-slip faulting history inferred from offsets of topographic features and basement rocks: a case study of the Arima-Takatsuki Tectonic line, southwest Japan. Tectonophysics 344, 81–101.
McGrath, A., Davison, G., 1995. Damage zone geometry around fault tips. J. Struct. Geol. 17, 1011–1024.
Miller, J.McL., Wilson, C.J.L., 2004. Structural analysis of faults related to a heterogeneous stress history: reconstruction of a dismembered gold deposit, Stawell, western Lachlan Fold Belt, Australia. J. Struct. Geol. 26, 1231–1256.
Minissale, A., Vaselli, O., Tassi, F., Magro, G., Grechi, G.P., 2002. Fluid mixing in carbonate acquifers near Rapolano (central Italy): chemical and isotopic constraints. Appl. Geochem. 17, 1329–1342.
Mollema, P.N., Antonellini, M., 1999. Development of strike-slip faults in the dolomites of the Sella Group, Northern Italy. J. Struct. Geol. 21, 273–292.
Molli, G., Cortecci, G., Vaselli, L., Ottria, G., Cortopassi, A., Dinelli, E., Mussi, M., Barbieri, M., 2009. Fault zone structure and fluid-rock interaction of a high angle normal fault in Carrara marble (NW Tuscany, Italy). J. Struct. Geol. doi:10.1016/j.jsg.2009.04.021.
Myers, R., Aydin, A., 2004. The evolution of faults formed by shearing across joint zones in sandstones. J. Struct. Geol. 26, 947–966.
Nemer, T., Meghraoui, M., 2006. Evidence of coseismic ruptures along the Roum fault (Lebanon): a possible source for the AD 1837 earthquake. J. Struct. Geol. 28, 1483–1495.
Odling, N.E., Harris, S.D., Knipe, R.J., 2004. Permeability scaling properties of fault damage zones in siliclastic rocks. J. Struct. Geol. 26, 1727–1747.
Pachell, M.A., Evans, J.P., 2002. Growth, linkage, and termination processes of a 10-km-long strike-slip fault in jointed granite: the Gemini fault zone, Sierra Nevada, California. J. Struct. Geol. 24, 1903–1924.
Passerini, P., 1964. Il Monte Cetona (Provincia di Siena). Boll. Soc. Geol. It 83, 219–238.
Peacock, D.C.P., Sanderson, D.J., 1992. Effects of layering and anisotropy on fault geometry. J. Geol. Soc. London 149, 793–802.
Peacock, D.C.P., 2001. The temporal relationship between joint and faults. J. Struct. Geol. 23, 329–341.
Peacock, D.C.P., Knipe, R.J., Sanderson, D.J., 2000. Glossary of normal faults. J. Struct. Geol. 22, 291–305.
Peacock, D.C.P., Sanderson, D.J., 1991. Displacements, segment linkare and relay ramps in normal fault zones. J. Struct. Geol. 13, 721–733.
Peacock, D.C.P., Sanderson, D.J., 1995. Strike-slip relay ramps. J. Struct. Geol. 17, 1351–1360.
Peccerillo, A., Poli, G., Donati, C., 2001. The Plio–Quaternary magmatism of southern Tuscany and northern Latium: compositional characteristics, genesis and geodynamic significance. Ofioliti 26, 229–238.
Petit, J.P., 1987. Criteria for the sense of movement on fault surfaces in brittle rocks. J. Struct. Geol. 9, 597–608.
Pollard, D.D., Aydin, A., 1988. Progress in understanding jointing over the past century. Geol. Soc. Am. Bull. 100, 1181–1204.
Pollard, D.D., Segall, P., 1987. Theoretical displacements and stresses near fractures in rock: with applications to faults, joints, veins, dikes, and pressure solution surfaces. In: Atkinson, B.K. (Ed.), Fracture Mechanics of Rock. Academic Press, London, pp. 277–349.
Rhodes, B.P., Perez, R., Lamjuan, A., Kosuwan, S., 2004. Kinematics and tectonic implications of the Mae Kuang fault, northern Thailand. J. Asian Earth Sci. 24, 79–89.
Riedel, W., 1929. Zur mechanic geologischer brucherscieinungnen. Zentral-blatt fur Mineralogie. Geologie Paleontologie B., 354–368.
Rodgers, D.W., Little, T.A., 2006. World's largest coseismic strike-slip offset: the 1855 rupture of the Wairarapa Fault, New Zealand, and implications for displacement/length scaling of continental earthquakes. J. Geoph. Res. Solid Earth 111 (B12), B12408.
Rossetti, F., Balsamo, F., Villa, I.M., Boujbauenne, M., Faccenna, C., Funiciello, R., 2008. Pliocene–Pleistocene HT/LP metamorphism during multiple granitic intrusions in the southern branch of the Larderello geothermal field (southern Tuscany, Italy). J. Geol. Soc. London 165, 247–262.
Rovida, A., Tibaldi, A., 2005. Propagation of strike-slip faults across Holocene volcano-sedimentary deposits, town of Pasto, Colombia. J. Struct. Geol. 27, 1838–1855.
Segall, P, Pollard, D, 1983. Nucleation and growth of strike slip faults in granite. J. Geoph. Res. 88B1, 555–568.
Serri, G., Innocenti, F., Manetti, P., 1993. Geochemical and petrological evidence of the subduction of delaminated Adriatic continental lithosphere in the genesis of the Neogene–Quaternary magmatism of central Italy. Tectonophysics 223, 117–147.
Sibson, R.H., 1977. Fault rocks and fault mechanism. J. Geol. Soc. London 133, 191–213.
Sibson, R.H., 1985. Stopping of earthquake ruptures at dilational fault jogs. Nature 316, 248–251.
Sibson, R.H., 1986. Rupture interaction with fault jogs. In: Das, S., Boatwright, J., Scholz, C.H. (Eds.), Earthquake Source Mechanics. Am. Geophys. Union, pp. 157–167.
Sibson, R.H., Robert, F., Poulsen, H., 1988. High angle reverse faults, fluid pressure cycling and mesothermal gold-quartz deposits. Geology 16, 551–555.
Sieh, K., Natawidjaja, D., 2000. Neotectonics of the Sumatran fault, Indonesia. J. Geophys. Res. 105, 28295–28326.
Stirling, M.W., Wesnousky, S.G., Shimazaki, K., 1996. Fault trace complexity, cumulative slip, and the shape of the magnitude-frequency distribution for strike-slip faults: a global survey. Geophys. J. Internat 124, 833–868.
Storti, F., Holdsworth, E.R., Salvini, F., 2003. Intraplate Strike-slip Deformation Belts. In: Geol. Soc. London, Spec. Publ., 210 1–14.
Storti, F., Rossetti, F., Läuferb, A., Salvini, F., 2006. Consistent kinematic architecture in the damage zones of intraplate strike-slip fault systems in North Victoria Land, Antarctica and implications for fault zone evolution. J. Struct. Geol. 28, 50–63.
Sylvester, A.G., 1988. Strike-slip faults. Geol. Soc. Am. Bull. 100, 1666–1703.
Tatar, O., Piper, J.D.A., Gursoy, H., Heimann, A., Kocbulut, F., 2004. Neotectonic deformation in the transition zone between the Dead Sea transform and the east Anatolian fault zone, southern Turkey: a palaeomagnetic study of the Karasu Rift volcanism. Tectonophysics 385, 17–43.
Tchalenko, J.S., 1970. Similarities between shear zones of different magnitudes. Geol. Soc. Am. Bull. 81, 1625–1640.

Tibaldi, A., Vezzoli, L., Pasquaré, F.A., Rust, D., 2008. Strike-slip fault tectonics and the emplacement of sheet–laccolith systems: the Thverfell case study (SW Iceland). J. Struct. Geol. 30, 274–290.

Van Der Zee, W., Wibbeley, C.A.J., Urai, J.L., 2008. The influence of layering and pre-existing joints on the development of internal structure in normal fault zones: the Lodéve basin, France. In: Wibberley, C.A.J., Kurz, W., Imber, J., Holdsworth, R.E., Collettini, C. (Eds.), The Internal Structure of Fault Zones: Implications for Mechanical and Fluid-Flow Properties, 299, pp. 57–74.

Ventura, G., Vilardo, G., Milano, G., Pino, N.A., 1999. Relationships among crustal structure, volcanism and strike–slip tectonics in the Lipari–Vulcano volcanic complex (Aeolian Islands, southern Tyrrhenian Sea, Italy). Phys. earth Planetary Interiors 116, 31–52.

Walker, R., Jackson, J., 2002. Offset and evolution of the Gowk fault, S.E. Iran: a major intra-continental strike-slip system. J. Struct. Geol. 24, 1677–1698.

Walker, R.T., Bayasgalan, A., Carson, R., Hazlett, R., McCarthy, L., Mischler, J., Molor, E., Sarantsetseg, P., Smith, L., Tsogtbadrakh, B., Thompson, G., 2006. Geomorphology and structure of the Jid right-lateral strike-slip fault in the Mongolian Altay mountains. J. Struct. Geol. 28, 1607–1622.

Wesnousky, S.G., 1988. Seismological and structural evolution of strike-slip faults. Nature 335, 340–342.

Wibberley, C.A.J., Shimamoto, T., 2003. Internal structure and permeability of major strike-slip fault zones: the Median Tectonic Line in Mie Prefecture, Southwest Japan. J. Struct. Geol. 25, 59–78.

Wilkins, S.J., Gross, M.R., Wacker, M., Eyal, Y., Engelder, T., 2001. Faulted joints: kinematics, displacement-length scaling relations and criteria for their identification. J. Struct. Geol. 23, 315–327.

Willemse, E.J.M., Pollard, D.D., 1998. On the orientation and patterns of wing cracks and solution surfaces at the tips of a sliding flaw or fault. J. Geoph. Res. 103, 2427–2438.

Woodcock, N.H., 1986. The role of strike-slip fault systems at plate boundaries. Phil. Trans. R. Soc. London A317, 13–29.

Wookcock, N., Schubert, C., 1994. Continental strike-slip tectonics. In: Hancock, P. (Ed.), Continental Deformation. Pergamon Press, New York, pp. 251–263.

Younes, A.I., Engelder, T., 1999. Fringe cracks; key structures for the interpretation of the progressive Alleghanian deformation of the Appalachian plateau. Geol. Soc. Am. Bull. 111, 219–239.